JGR Planets

RESEARCH ARTICLE
10.1029/2023JE008242

An Orbital Comparison of a Late Mantling Unit on Aeolis Mons With Other Erosion-Resistant Strata Explored by MSL in Gale Crater, Mars

A. Rudolph[1,2], B. Horgan[1], K. Bennett[3], C. Weitz[4], R. Sheppard[4,5], S. G. Banham[6], A. B. Bryk[7], E. Kite[8], A. Roberts[6], and L. Scuderi[9]

[1]Department of Earth, Atmospheric, and Planetary Sciences, Purdue University, West Lafayette, IN, USA, [2]Center for Earth and Planetary Studies, National Air and Space Museum, Smithsonian Institution, Washington, DC, USA, [3]U.S. Geological Survey, Astrogeology Science Center, Flagstaff, AZ, USA, [4]Planetary Science Institute, Tucson, AZ, USA, [5]Institut d'Astrophysique Spatiale, Université Paris-Saclay, Orsay, France, [6]Department of Earth Science and Engineering, Imperial College London, London, UK, [7]Department of Earth and Planetary Science, University of California, Berkeley, CA, USA, [8]Department of Geophysical Sciences, University of Chicago, Chicago, IL, USA, [9]Earth and Planetary Science Department, Institute of Meteoritics, University of New Mexico, Albuquerque, NM, USA

Key Points:

- A newly mapped mantling unit has surface and spectral features similar to the marker band, both of which differ from the surrounding strata
- The mantling unit may represent a similar depositional and/or alteration environment as the marker band but much later in geologic time
- The marker band, mantling unit, and mound skirting unit may have similar sediment sources but different water interactions after deposition

Supporting Information:

Supporting Information may be found in the online version of this article.

Correspondence to:

A. Rudolph,
rudolph4@purdue.edu;
rudolpha@si.edu

Citation:

Rudolph, A., Horgan, B., Bennett, K., Weitz, C., Sheppard, R., Banham, S. G., et al. (2024). An orbital comparison of a late mantling unit on Aeolis Mons with other erosion-resistant strata explored by MSL in Gale crater, Mars. *Journal of Geophysical Research: Planets*, *129*, e2023JE008242. https://doi.org/10.1029/2023JE008242

Received 19 JAN 2024
Accepted 29 JUN 2024

Abstract Previous investigations along *Curiosity*'s traverse in Gale crater have explored the relationship between orbital and in situ observations. This work aims to better understand the geologic environment of units only observable from orbit and compare them to the properties of units examined by *Curiosity*. Here, we map an erosion-resistant dark-toned mantling unit that overlies the modern topography of Aeolis Mons (informally known as Mt. Sharp) and compare this unit to two other previously mapped dark-toned resistant units, the marker band and the mound skirting unit (MSU), that have been inferred to represent different geologic environments (lacustrine and aeolian, respectively). Visible to short wave infrared spectra from the Compact Reconnaissance Imaging Spectrometer for Mars and visual images from the High Resolution Imaging Science Experiment and Context Cameras aboard the Mars Reconnaissance Orbiter are used for this comparison. Spectral data suggest a mafic composition with minor alteration, although the composition varies more with location around Mt. Sharp rather than between units. Morphologically, the mantling unit has strong similarities to the marker band based on their consistent low-albedo, erosion-resistance, and smooth appearance, contrasting with the highly variable surface texture of the MSU. We hypothesize that all three units had a similar sediment source but experienced aqueous alteration at different times: early ubiquitous cementation in a surface aqueous environment in the mantling unit and marker band versus patchy late diagenesis in the MSU. If true, these results suggest that water activity continued within the Gale crater long after the erosion of Mt. Sharp.

Plain Language Summary Mars *Curiosity* rover observations of the physical and chemical properties of rocks are used to characterize past geologic environments in Gale crater. Here, we aim to constrain the properties of geologic units inferred to have formed from past lake and sand dune environments using satellite data sets to see if these same environments can be identified elsewhere on Mars. A newly mapped mantling unit is compared, which overlies (or mantles) rocks in Gale crater, representing deposition later in time. We use compositional data from the Compact Reconnaissance Imaging Spectrometer for Mars and images from the High Resolution Imaging Science Experiment and Context Cameras all aboard the Mars Reconnaissance Orbiter to identify the properties of units in this study. We find that although the mantling unit has a similar composition to both the inferred lake (marker band unit) and sand dune (mound skirting unit) environments, its physical appearance is more similar to the marker band lake environment. This suggests that the mantling unit may represent a water environment and has important implications for understanding the timing of when water was present on Mars.

1. Introduction

Important constraints on the climate history of ancient Mars can be obtained from the rocks that are observed at the surface. Understanding the climate at the time of deposition and subsequent alteration of sedimentary rock outcrops is one of the main goals of the Mars Science Laboratory (MSL) *Curiosity* rover mission that landed on the northwestern floor of the ~154-km diameter Gale crater (Grotzinger et al., 2012). The fluvial, lacustrine, and aeolian deposits at the base of the ~5 km high Aeolis Mons (informally known as "Mt. Sharp") in Gale crater are

layered, recessive, variable in albedo, and exhibit signatures in orbital reflectance spectra that are dominated by secondary minerals, including hematite, clay minerals, and sulfates (e.g., Fraeman et al., 2016; Sheppard et al., 2021). However, Mt. Sharp also includes geologic units that do not show clear signs of aqueous alteration from orbit and are instead spectrally dominated by mafic minerals. These include: active dune fields (e.g., Lapôtre et al., 2017), the mound skirting unit (MSU; e.g., Sheppard et al., 2021) and a late aeolian sandstone that drapes lower Mt. Sharp (R. Anderson & Bell, 2010; Banham et al., 2018); the marker band, a distinct dark-toned and smooth bench-forming layer within the Mt. Sharp stratigraphy (Milliken et al., 2010; Sheppard et al., 2021; Weitz et al., 2022); and the mantling unit that drapes upper Mt. Sharp—newly mapped in this study. In this study, we compare the MSU, the marker band, and the mantling units to better understand their origin interpreted from orbit and the implications of these units for the geologic history of Gale crater.

The MSU is a widespread low-lying erosion-resistant unit first mapped by R. Anderson and Bell (2010) and visited by *Curiosity* in several locations throughout the MSL mission. The area of the MSU visited by *Curiosity*, known as the Stimson formation within the Siccar Point group, is interpreted to have formed through aeolian processes and is a diagenetically altered sandstone that records aeolian dune migration (e.g., Banham et al., 2018, 2021, 2022; Bedford et al., 2020, 2022; Frydenvang et al., 2017; Yen et al., 2017).

The marker band, previously named the "marker bed" or "marker horizon" is a laterally extensive dark toned, smooth textured, and bench-forming unit that is morphologically distinct relative to its surroundings but appears confined within the Mt. Sharp stratigraphy (Milliken et al., 2010; Weitz et al., 2022). The leading hypotheses for the origin of this layer prior to the in situ investigation were formation as an indurated sulfate or through processes that did not require water (i.e., impacts, volcanism, or aeolian processes), which have distinct climatic implications that suggest a dry period in Gale crater (Fraeman et al., 2016; Milliken et al., 2010; Weitz et al., 2022). Because the marker band occupies an important stratigraphic location just above the boundary of the clay-mineral dominated strata of lower Mt. Sharp and the sulfate-dominated strata of upper Mt. Sharp (Milliken et al., 2010), a better understanding of the origin of the marker band is important for reconstructing the geologic and climatic history of Gale crater.

We use a combination of grayscale images from the High Resolution Imaging Science Experiment (HiRISE; McEwen et al., 2007) and the Context Camera (CTX; Malin et al., 2007) and visible, near-infrared, and shortwave infrared (VNIR/SWIR; 0.7–2.65 μm) hyperspectral cubes from the Compact Reconnaissance Imaging Spectrometer for Mars (CRISM; S. Murchie et al., 2007) to evaluate the morphology, distribution, and composition of exposures of interest of the mantling unit and compare these properties to what is observed in the marker band and the MSU. The results will contribute to the present understanding of the timing and heterogeneity of different geologic processes that occurred in the Gale crater. This study will also help us better understand how geologic interpretations from in situ exploration can be applied more broadly to Mt. Sharp. For example, if rover data demonstrate that the marker band and the MSU represent distinct environments, to what extent can differences in their orbital properties be used to distinguish similar environments? This will help to provide context for future orbital studies both in the Gale crater and potentially elsewhere on Mars.

2. Background

2.1. Mt. Sharp Stratigraphy From Orbit

Mt. Sharp is located within the Gale crater and is composed of a ∼5 km thick stratigraphic record that spans multiple geologic eras (Thomson et al., 2011). From the orbit, the lower strata of Mt. Sharp appear compositionally dominated by crystalline Fe-oxides and clay minerals, indicative of a wet environment, that transitions at higher elevations to strata dominated by sulfate minerals, indicative of a drier environment (e.g., Fraeman et al., 2016; Milliken et al., 2010). The marker band is observed within the stratigraphy of Mt. Sharp near the clay-sulfate transition boundary (Figure 1a; Milliken et al., 2010). Based on orbital data, the dominant hypotheses for the type of deposit that the marker band represents include deposits of indurated sulfate, aeolian sediments, volcanic ash, and/or lag deposits (e.g., Weitz et al., 2022).

The previously mapped MSU drapes lower Mt. Sharp at elevations ranging from −4,070 to −1,140 m and is described as a pitted mesa-forming unit with parallel ridges at some locations (R. Anderson & Bell, 2010). In some regions, the surface of the MSU is described as a washboard unit, which refers to the visual surface texture that results from the preservation of interdune materials by the erosion of dune crests (Milliken et al., 2014). The

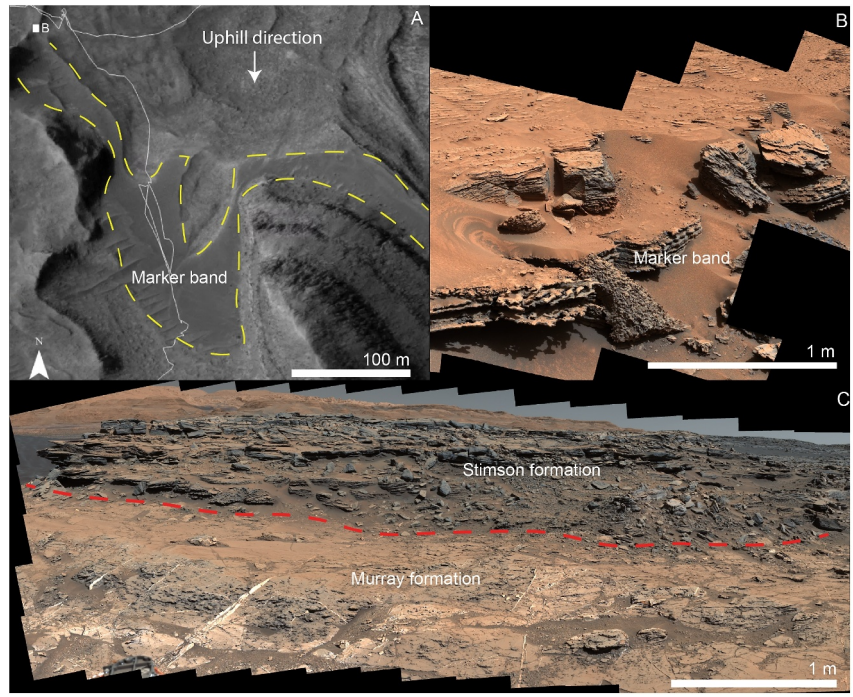

Figure 1. Images of the marker band from orbital (a) and rover (b, c) perspectives. (a) Orbital view of the marker band from High Resolution Imaging Science Experiment image ESP_02869_1755_RED. Curiosity's traverse is denoted by the white line and approximate marker band location is outlined by the yellow dashed lines. (b) Mastcam natural color mosaic of the marker band shown eroding onto the sediment covered slope, Sol 3689 mcam 34 mm seqid mcam03304. (c) Mastcam natural color mosaic of the Stimson formation (east side of Naukluft plateau) overlying the Murray formation, with the approximate boundary location denoted by the red dashed line, Sol 1275 mcam 34 mm seqid mcam05976.

MSU has also been described as a "higher thermal inertia" (TI) unit with thermal inertia values ranging from ~450 to 550 J m^{-2} K^{-1} $s^{-1/2}$, whereas most of the lower stratigraphy of Mt. Sharp ranges from 300 to 400 J m^{-2} K^{-1} $s^{-1/2}$ (Fraeman et al., 2016). CRISM albedo of the higher TI unit ranges from 0.20 ± 0.01, comparable to surrounding units that range from 0.19 ± 0.02 to 0.25 ± 0.05 (Fraeman et al., 2016), and a CTX albedo of 0.16–0.21 (R. Anderson & Bell, 2010). From orbit, this unit was hypothesized to be either fluvial or aeolian in origin (R. Anderson & Bell, 2010).

The mantling unit has not been specifically mapped to the same extent as described in this study but does partly overlap with previous mapping of mantling units. Other similar units mapped from orbit in Gale include the "thin mantle unit" that is described to have a "feathery" erosional expression, but examples shown in R. Anderson and Bell (2010) do not all have a smooth appearance that is consistent with the mantling unit discussed here. The "thin mantle unit" is observed at elevations ranging from −4,070 to −1,140 m and has a CTX albedo of 0.20–0.23. Another unit, the "dark-toned layered yardangs," is observed at elevations ranging from −4,460 to −1,800 with a CTX albedo of 0.18–0.22 and is described as having thin layers of varying properties that form large yardangs (R. Anderson & Bell, 2010). While the yardangs are not a mantling unit, a large portion of the newly mapped mantling unit overlaps the "dark-toned layered yardangs."

2.2. Mt. Sharp Stratigraphy From In Situ Exploration

Curiosity's in situ exploration of lower Mt. Sharp has shown that the dominant depositional environment is a combination of fluvial, lacustrine, and aeolian (e.g., Grotzinger et al., 2014; Rapin et al., 2021). However, the duration, frequency of recurrence, and spatial extents of these environments remain unclear (e.g., Grotzinger et al., 2014; Palucis et al., 2016; Stack et al., 2014). The stratigraphy of lower Mt. Sharp explored by *Curiosity* is divided into three groups: the Bradbury, Mt. Sharp, and Siccar Point groups (Fraeman et al., 2016; Grotzinger et al., 2015; Siebach et al., 2017), the latter two of which are relevant to this study.

The Mt. Sharp group represents the majority of lower Mt. Sharp and is composed of altered fluvial, lacustrine, and aeolian sediments. At elevations below −3,850 m, it has been divided in relative stratigraphic order from lower to higher elevations into the Murray, Carolyn Shoemaker, and Mirador formations (Fedo et al., 2022; Grotzinger et al., 2015; Gupta et al., 2022; Rapin et al., 2021). The Murray formation is a >400 m thick package of mudstones and sandstones (Figure 1c) and has been interpreted by the MSL team to represent a more perennial, low energy, lacustrine environment (e.g., Edgar et al., 2020; Fedo et al., 2022; Grotzinger et al., 2015). The Carolyn Shoemaker formation is dominated by fine- to medium-grained sandstones and is interpreted to record interactions between fluvial and lacustrine environments (Fedo et al., 2022). The Mirador formation is composed of large-scale cross-stratified sandstones interpreted to be large, migrating aeolian dunes intercalated with evidence for transient ponds as indicated by ripple structures in interstratified lenses within the sandstone facies (Gupta et al., 2022; Roberts et al., 2023).

The Siccar Point group is the rover-explored component of the orbitally defined and regionally extensive MSU. The unconformity delineating the Mt. Sharp group and the Siccar Point group stratigraphy is defined as the basal Siccar Point group unconformity and has been mapped along the traverse by Watkins et al. (2022). Mapped along the rover traverse, the unconformity cross-cuts approximately 450 m of Mt. Sharp group stratigraphy (Banham et al., 2022; Watkins et al., 2022). The basal unit within the Siccar Point group—the Stimson formation—is an aeolian sandstone unit that unconformably overlies the Mt. Sharp group, deposited after the exhumation of Mt. Sharp and represents a predominantly dry period in Gale crater and forms a resistant cap, expressed as plateaus (Emerson and Naukluft), isolated buttes (Murray Buttes, Lobster mountain, Ireson Hill) and pediment-capping units (Greenheugh) at several locations along *Curiosity*'s traverse (e.g., Banham et al., 2018, 2021, 2022; Bedford et al., 2020, 2022; Fraeman et al., 2016; Watkins et al., 2022). The Stimson formation, currently the only rover-observed formation in the Siccar Point group, is dominated by mafic sandstones (Figure 1c; Bedford et al., 2020, 2022). Although the stratigraphy records primarily deposition within an arid aeolian environment, exposures show evidence for some post-deposition aqueous activity. Ca-sulfate veins and cement, fracture associated halos, and concretions are observed in the Emerson and Naukluft plateaus (Bedford et al., 2020; Frydenvang et al., 2017; Kronyak et al., 2019; Sun et al., 2019; Yen et al., 2017) and light- and dark-toned alteration veins are present in the Greenheugh pediment (Gasda et al., 2022; Rudolph et al., 2022), all of which are part of the Stimson formation. Aqueous fluid leaching of elements, likely through subsurface fluids, is observed in altered portions of the Stimson formation (Yen et al., 2017). Finally, sedimentary structures consistent with soft sediment deformation are observed in the Greenheugh pediment and are largely restricted to the eastern margin (Banham et al., 2023; Dietrich et al., 2022).

2.3. The Marker Band

Previous marker band orbital analyses describe the following morphologic features: low albedo, erosion resistant, and smooth, all relative to surrounding units (Figure 1a; Fraeman et al., 2016; Milliken et al., 2010; Sheppard et al., 2021; Weitz et al., 2022). VNIR/SWIR CRISM analyses show that the dominant orbital composition of the marker band has spectral features consistent with mafic minerals, primarily high-Ca pyroxene (Weitz et al., 2022) with some regions, predominantly in eastern Mt. Sharp, where the layer is spectrally neutral (i.e., lacking diagnostic spectral features; Sheppard et al., 2021; Weitz et al., 2022). Previous orbital studies interpret the marker band as a single layer that was at one point continuous across Mt. Sharp prior to eroding to its current exposures or alternatively formed through local events at multiple locations across Mt. Sharp (Weitz et al., 2022). Marker band exposures across Mt. Sharp dip away from the central peak by 1°–5°, which could be consistent with a single layer across Mt. Sharp, but multiple layers forming contemporaneously in different regions cannot be ruled out (R. B. Anderson et al., 2018; Kite et al., 2016; Milliken et al., 2010; Sheppard et al., 2021; Weitz et al., 2022).

The *Curiosity* rover investigated the marker band in situ during 2022–2023. The morphology of the lower marker band observed by *Curiosity* in situ consists of lithified centimeter-scale symmetric ripples indicative of a shallow water environment (Dietrich et al., 2023; Gasda et al., 2023; Gupta et al., 2023; Weitz et al., 2023). This wet environment interpretation was not anticipated based on orbital studies, highlighting a gap in understanding the outcrop and orbital expression of this particular type of environment on Mars.

2.4. Mapping Intent

This work utilizes CRISM VNIR/SWIR hyperspectral image cubes and HiRISE and CTX grayscale images to characterize the spectral and morphologic properties of the MSU, the marker band, and the mantling unit. The mantling unit, as mentioned previously, is a newly mapped unit described herein for the first time. The marker band has been mapped previously (e.g., Milliken et al., 2010; Sheppard et al., 2021; Weitz et al., 2022); our map includes possible additional indurated, bench-forming layers within the stratigraphy. We use existing mapped exposures of the MSU (R. Anderson & Bell, 2010). The aeolian MSU and lacustrine marker band have been visited by MSL, but the mantling unit has not. A goal of this work is to take what we have learned from in situ exploration to explain the orbital signatures from the MSU and marker band and then attempt to apply that to sites a rover will not examine. If we can determine specific differences such as unique textures or compositions through orbital properties of the MSU, a dominantly aeolian unit, compared to the marker band, a lacustrine unit, and the mantling unit of unknown origin, we can help inform the origin of the mantling unit and determine whether they all formed at different times and temporal locations throughout the history of Mt. Sharp. Measurables, based on previous studies, include the relative smoothness, albedo, resistance to erosion, layer tilt (within or overlying stratigraphy), and composition (e.g., Edgett & Sarkar, 2021; Malin & Edgett, 2000; Milliken et al., 2010; Sheppard et al., 2021; Weitz et al., 2022).

If the mantling unit has a similar composition and morphology to the marker band, we hypothesize that the process that formed the marker band is a repeating depositional and/or diagenetic process occurring at least once within stratigraphy (the marker band) and once after Mt. Sharp had undergone significant erosion (the mantling unit). If these units do not have similar orbital properties, we hypothesize that they formed in different depositional environments (e.g., aeolian, impact-related, or volcanic) and/or through different late-stage processes (e.g., burial, lithification, and diagenesis). If morphology and composition properties are variable (e.g., similar compositions but different morphologies), similar compositions could suggest a similar sediment source and/or alteration history, whereas similar morphology could suggest a similar depositional process and/or alteration history.

3. Methods

3.1. Morphology

We used high resolution (0.26 m/pixel) HiRISE grayscale images (McEwen et al., 2007) to qualitatively map the distribution of the original marker band and morphologically similar units on Mt. Sharp across 69 images that cover most of Mt. Sharp (Table S1 in Supporting Information S1). Using ArcGIS Pro, HiRISE images were manually georeferenced to a Gale crater mosaic created from 6 m/pixel CTX images (Malin et al., 2007). Features used to identify the marker band and similar unit exposures include a low relative albedo (i.e., relatively dark in appearance compared to surrounding units), a smooth and lithified surface, where lithification was determined by the preservation of a crater on the unit's surface, and whether the unit has a bench-forming morphology. Exposures were manually mapped using the described features mapped with the polyline feature tool in ArcGIS Pro. Elevations were extracted from a High-Resolution Stereo Camera (HRSC) 50 m resolution digital terrain model (DTM) of the study area (Fergason et al., 2018; Neukum et al., 2004). HiRISE DTMs made from HiRISE stereo image pairs were used to determine layer tilt in select areas. The MSU was mapped by R. Anderson and Bell (2010), and although we conducted a fresh analysis of the morphology of the MSU, we used their work as the basis for our investigation and did not attempt to extend this previous mapping effort.

3.2. Composition

We used VNIR/SWIR (0.4–2.65 μm) hyperspectral image cubes from CRISM (S. Murchie et al., 2007) to constrain the composition of the units identified in visible images. The wavelength range of the CRISM instrument is sensitive to iron in minerals and can be used to differentiate primary igneous minerals as well as Fe/Mg/Al-silicates, -sulfates, and -clay minerals (S. Murchie et al., 2007). All cubes analyzed are in full resolution targeted mode with a spatial resolution of ∼18 m/pixel and spectral resolution of 6.55 nm/channel (S. Murchie et al., 2007).

Map-Projected Targeted Reduced Data Record (MTRDR) and Target Reduced Data Record (TRDR) version 3 cubes were used to maximize the spatial coverage as MTRDR coverage is limited in relevant areas for this study

(see Table S2 in Supporting Information S1). MTRDR cubes are initially processed with a basic photometric correction for Lambertian scattering, a "volcano scan" correction for atmospheric CO_2, and are map projected using martian surface terrain models (Bibring et al., 1989; Langevin et al., 2005; McGuire et al., 2009; F. P. Seelos et al., 2016, 2023). TRDR cubes contain data calibrated to radiance and need to be further processed by the user to estimate Lambert albedo using Interactive Data Language (IDL) and Environment for Visualizing Images (ENVI; S. Murchie et al., 2007). Separate data files for the VNIR and SWIR sensors are available on the Planetary Data System (PDS) Geosciences Node. Using the CRISM Analysis Toolkit (CAT) 7.4 for ENVI, TRDR cubes were processed by: (a) converting the file format from PDS to CAT, (b) converting radiance to I/F (radiance/solar flux) adjusted to Mars distance, and (c) atmospheric corrections by division by scaled volcano observation (S. Murchie et al., 2007). TRDR cubes were then imported into IDL and with the Derived Data Record files from the PDS, latitude and longitude data were used to map and join the data from the VNIR and SWIR sensors.

MTRDR and processed TRDR cube spectra were compared with spectrally neutral terrains in order to highlight subtle spectral features that would otherwise be overshadowed by noise or martian dust. Ratios for MTRDR cubes followed the procedure outlined by Horgan et al. (2020) using the R770 parameter from Viviano et al. (2014). An average of all neutral pixels in the cube is then used to create a neutral reference spectrum used to ratio the entire cube. TRDR cube spectra require a manually selected dusty spectrum region of interest (ROI) to be used for ratioing each spectrum used; this was done using the Spectral Math feature in ENVI.

MTRDR and TRDR spectra shown in this paper are averages from pixels in a single ROI manually selected in ENVI, smoothed using a boxcar average with a width of 6 CRISM channels, and de-spiked with a tolerance of 0.003. ROIs were selected based on the locations of the mapped exposures of the relevant units in this study. Due to the combination of the spatial resolution of CRISM images and the small exposures of some units, ROI size varies from 9 to 1,480 pixels (see Table S3 in Supporting Information S1). In general, the larger the ROI, the higher quality spectrum is produced because spectral noise is more likely to average out. As a result, for small ROIs, some of the spectra are noisy and have higher uncertainties. However, they are used because they are in areas of high interest (primarily marker band exposures). A small narrow reflectance peak or band near 1.2 μm is present in some spectra; this is a noise artifact (S. Murchie et al., 2007).

Mafic mineral spectral parameters were calculated in IDL on extracted ratio spectra to help visualize compositional trends and quantify specific band absorption features. Parameters used include 1 μm band center, 2 μm band center, band area for 1 and 2 μm, and the ratio of the 1 μm /2 μm bands. Band parameters were calculated following the procedures outline by Horgan et al. (2014). Spectral features near 1 and 2 μm can differentiate between primary mafic minerals and basaltic glass (Figure 2; Adams, 1968; Horgan et al., 2014; Viviano et al., 2019). Olivine has a broad, deep, and asymmetrical triplet absorption centered between 1.05 and 1.07 μm (Adams, 1968; Cloutis & Gaffey, 1991; King & Ridley, 1987). High-Ca pyroxene most commonly exhibits two broad and symmetrical absorptions centered between 0.98–1.05 and 2.10–2.40 μm, while low-Ca pyroxene exhibits similar absorptions centered between 0.90–0.93 and 1.9–2.0 μm (Adams, 1974; Cloutis & Gaffey, 1991; Klima et al., 2007, 2011). Basaltic glass has a shallow, broad, symmetrical absorption centered between 1.07 and 1.15 μm and between 1.90 and 2.10 μm if Fe^{3+} is present (Cloutis et al., 1990; Horgan et al., 2014).

Alteration minerals were identified based on the presence of narrow absorption bands between 1.4 and 2.5 μm (Figure 2). All clay and hydrated sulfate minerals can have absorptions between 1.39–1.46 and 1.91–1.97 μm respectively associated with OH^- and H_2O (Bishop et al., 1994, 2008; Cloutis et al., 2006). Shape and depth can vary from a narrow singlet, more common in clay minerals, to a broader doublet or triplet more common in sulfates (Bishop et al., 1994, 2008; Cloutis et al., 2006). Fe-/Mg-clay minerals have a narrow absorption band centered at 2.29–2.37 μm (Bishop et al., 2008). Al-clay minerals and hydrated silica have either a single or a doublet narrow absorption at 2.17–2.21 μm (Bishop et al., 2008). Monohydrated sulfates have a narrow absorption at 2.4 μm that is associated with $(SO_4)^{2-}$ stretching vibrations (Cloutis et al., 2006). Polyhydrated sulfates (PHS) have a drop in reflectance at wavelengths greater than ~2.3–2.4 μm and $Fe^{2+/3+}$ can display an absorption band centered between 0.8 and 0.95 μm, sometimes as a broad doublet with an additional band centered at 1.17 μm.

Residual spectral absorptions due to the martian atmosphere are present between 1.9 and 2.1 μm (S. L. Murchie et al., 2009). To minimize the effects of both the noise in the spectra and the residual absorptions due to the martian atmosphere, a fourth order polynomial fit was conducted on select spectra prior to parameterization (see Figure S1 in Supporting Information S1). This correction was only performed on spectra that were qualitatively

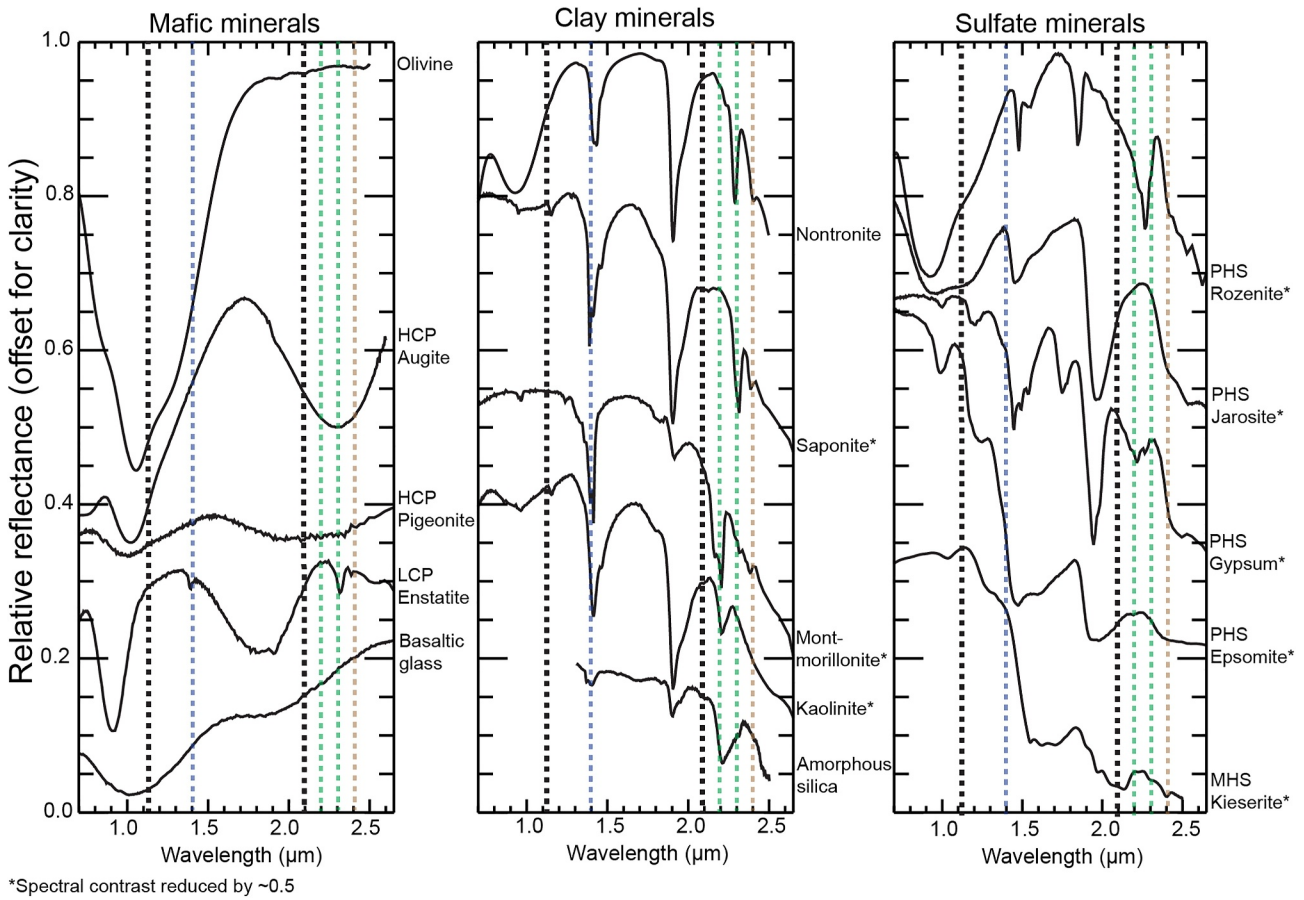

Figure 2. Laboratory spectra of relevant mafic (left), clay (middle), and sulfate (right) minerals. Dashed lines indicate features of interest for typical marker bands (black), hydration (blue), clays (green), and sulfates (tan). Spectra are from the USGS Spectral Library Version 7 (Kokaly et al., 2017) and the University of Winnipeg's Center for Terrestrial and Planetary Exploration's spectral database.

dominated by 1 and 2 μm absorptions as any other absorptions are lost in the fitting process. The fit spectra were then continuum removed (e.g., Clark & Roush, 1984) and parameter calculations were conducted in IDL.

4. Results

4.1. Morphology and Distribution of the Marker Band and Related Units

The marker band has previously been defined as a smooth, low-albedo, and erosion-resistant layer within the Mt. Sharp stratigraphy (e.g., Milliken et al., 2010; Figure 1a). Here, we use that definition for identification of and comparison to other similar morphologic units on Mt. Sharp. Based on our mapping efforts, we have identified four categories of morphologic units, as discussed in more detail below: (1) marker band and other low-albedo bench-forming layers, (2) high-albedo bench-forming unit, (3) mantling unit, and (4) MSU (Figure 3).

4.1.1. The Marker Band and Other Low-Albedo, Bench-Forming Layers

Exposures of the marker band with the typical low-relative-albedo, erosion-resistant, and a topographically smooth appearance on a 10 s of meters-scale are observed within the strata that constitute Mt. Sharp extending from the northwest region where MSL is exploring to the southwest (Figures 3, 4a–4c, and 4h). Our mapping of this unit largely agrees with that of Weitz et al. (2022). However, we observe additional layers that are bench-forming and indurated within the stratigraphy of Mt. Sharp at a similar elevation as the marker band, but they are observed at slightly higher and/or lower elevations than marker band exposures within the same HiRISE image (Figures 4a, 4c, and 4h). This includes at least one additional nearby layer within the stratigraphy that is also partially consistent with the typical marker band (Figures 4a, 4c, and 4h). These layers are not quite as smooth

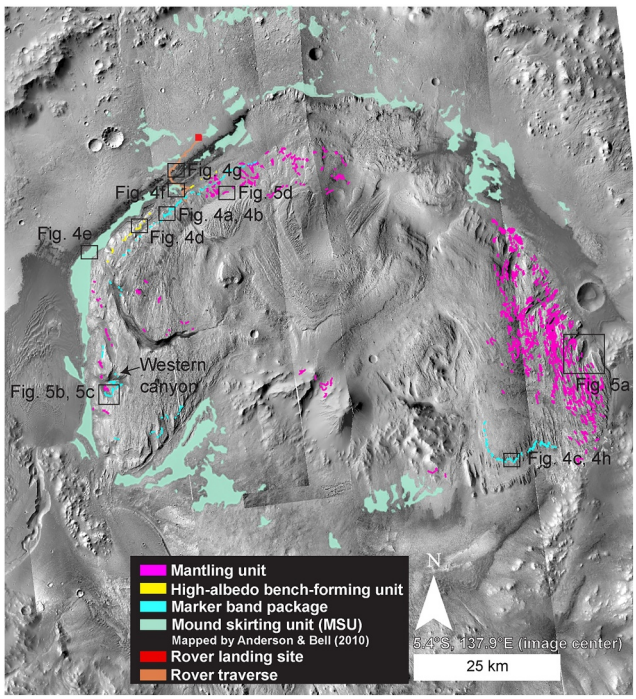

Figure 3. Context Camera mosaic of mapped exposures of marker band packages, the high-albedo bench-forming unit, and the mantling unit along with mound skirting unit polygons from R. Anderson and Bell (2010). Lines are located at the bench-side of each marker band layer or surrounding exposures of the mantling unit.

but are still erosion resistant benches with relatively low albedo compared to surrounding layers. We categorize these layers in the same morphologic unit as the marker band and refer to them (including the marker band) as a marker band "package" rather than a singular marker band layer. However, we cannot rule out that while similar in appearance, these layers are unrelated to the marker band.

The NW package contains the well-studied marker band along *Curiosity's* traverse as well as two additional layers in the package, one stratigraphically above and one below the marker band (Figure 4a). While the marker band is one long, fairly continuous layer with a lateral extent of ∼24 km as traced from northwest Mt. Sharp into the western canyon, the additional layers mapped are only observed in small lateral extents (10 s of meters). The approximate elevation range of the NW package is from −3,890 to −3,550 m.

The SW layer outcrops as a single clear layer (Figure 4b) that is overall consistent with the mapping of Weitz et al. (2022). This layer is also indurated, bench-forming and smooth at 10 s of meter scale with a relatively low albedo. The approximate elevation range of the SW layer is from −3,300 to −2,500 m. The discontinuous lateral extent of the exposed SW layer is approximately 16.5 km, as traced around the western lobe of Mt. Sharp.

The SE package has one main layer similar in morphology to the marker band and up to five additional bench-forming low-albedo but less smooth layers embedded within the stratigraphy below (Figures 4c and 4h). There is a large, mottled region horizontally separating the main marker band layer and the lower layers. Approximate elevation ranges for SE package layers are −2,630 to −2,750 m for the main layer, and −2,850 to −2,800 m for the lower layers. The discontinuous lateral extent of the exposed SE package layers is ∼13 km.

4.1.2. The High-Albedo Bench-Forming Unit

The high-albedo bench-forming unit is a single layer that has a higher relative albedo and rougher texture than the typical marker band, but it also exhibits bench-forming outcrop exposures. Sediments that appear to be eroded from or collected at the base of this unit have a low albedo (Figure 4d). This unit is only observed in the northwest region of Mt. Sharp and is stratigraphically lower than the main marker band of the NW package (Figure 3). The approximate elevation range for this unit is from −4,080 to −4,030, and the unit has a 12 km lateral extent that can be traced across northwest Mt. Sharp.

4.1.3. The Mound Skirting Unit

The MSU, as previously mapped by R. Anderson and Bell (2010), is observed near the base of Mt. Sharp as shown in Figure 3 and is most prominent on its western slopes. It is possible that additional exposures on the eastern side are now covered by the large dune field but that cannot be confirmed. The elevation range of this unit is ∼−4,530 to −3,100 m, and the lateral extent of exposures is ∼208 km around the base of Mt. Sharp. The MSU exhibits variable and inconsistent morphologies (Figures 4e–4g) with typical MSU exposures around Mt. Sharp exhibiting varying albedos. However, higher relative albedos are more common than lower albedos. The MSU appears mottled in the Naukluft plateau region (Figures 3 and 4g) but slightly less mottled in most other exposures and at the Greenheugh pediment (Figures 3, 4e, and 4f). The MSU also shows variable resistance to erosion. Endmembers include the Naukluft Plateau, which does not appear to be particularly resistant to erosion, and the Greenheugh pediment, which is erosion resistant. The MSU around the rest of Mt. Sharp appears to be somewhere in between these two endmembers and in some exposures exhibits a washboard surface texture (Milliken et al., 2014).

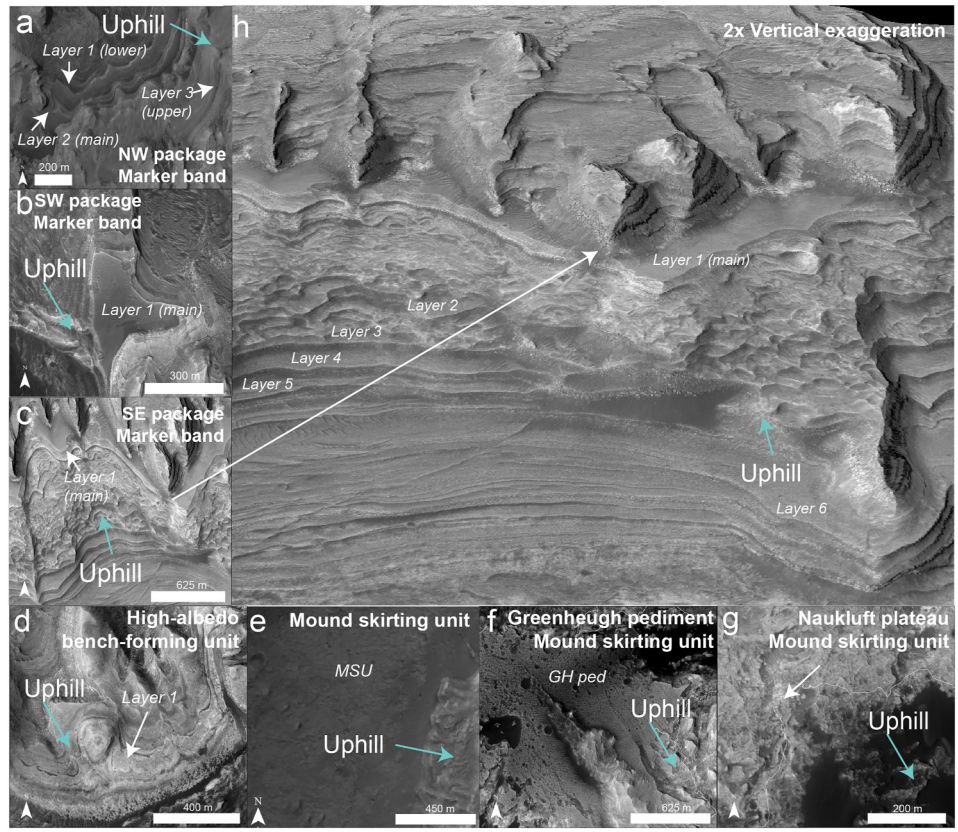

Figure 4. High Resolution Imaging Science Experiment (HiRISE) images of (a–c) marker band packages, ESP_019988_1750_RED, ESP_013540_1745_RED, and ESP_014186_1745_RED, (d) high albedo bench-forming layer, ESP_012847_1750_RED (e–g) mound skirting unit ESP_017008_1750_RED and ESP_039280_1755_RED_C_01_ORTHO, and (h) HiRISE digital terrain model with 2× vertical exaggeration of the SE Package marker band layers.

4.1.4. The Mantling Unit

The mantling unit has a low relative albedo, smooth appearance, and resistance to erosion similar to the typical marker band, but rather than forming distinct benches that are confined by stratigraphic layers, this unit mantles existing stratigraphy (Figure 5). This unit is observed at multiple locations across Mt. Sharp but none directly in the path of *Curiosity* (Figure 3). The most prominent exposure of the mantling unit is on eastern Mt. Sharp where most analyses are focused. The unit is relatively flat overlying existing topography in large eastern Mt. Sharp exposures that surround the dark-toned layered yardangs identified by R. Anderson and Bell (2010) and continue downslope into valleys in northeastern Mt. Sharp. The unit crops out as a large patch of connected planar exposures with inliers exposing a more mottled underlying surface. The approximate elevation range for the eastern exposure of this unit is from −4,155 m at the base of valley mouths and −2,130 m at the top of the flat lying region. The flat lying region of this exposure (~420 km^2) ranges from approximately −2,800 to −2,130 m in elevation (Figure S2 in Supporting Information S1). While there are a higher number of smaller exposures in northern Mt. Sharp near MSL, the largest singular outcropping of this unit beyond eastern Mt. Sharp is in southwestern Mt. Sharp (Figures 5b and 5c). The presence of abundant sand and its location on a slope make it difficult to determine whether this unit was deposited as a singular mantling-like unit or as many smaller marker band-like layers. However, analysis of the DTM clearly shows that this exposure does mantle existing topography (Figure 5c) and that the mantling unit exposures have a steeper layer tilt than the underlying strata. The approximate elevation range for this exposure is −3,453 to −2,980 m (Figure S2 in Supporting Information S1) and the approximate area is 1.8 km^2 although at least half of this area is sand covered. Smaller exposures of the mantling unit are present in north Mt. Sharp and have a "feathery" appearance (Figure 5d) that is consistent with the "thin mantle unit" exposures from R. Anderson and Bell (2010). These patchy exposures have a lateral extent

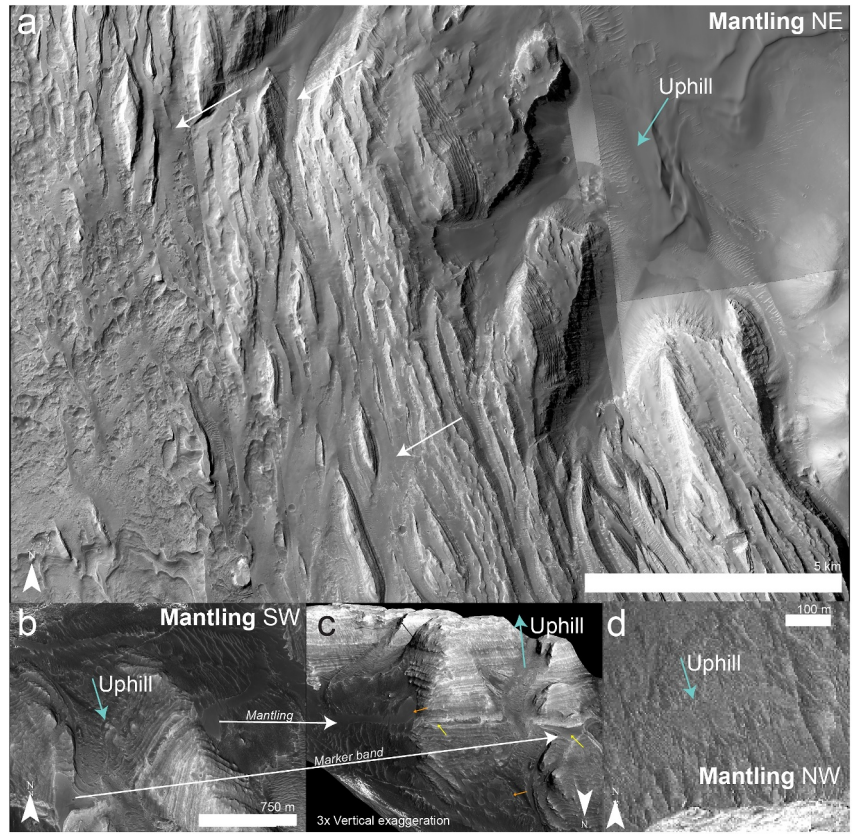

Figure 5. High Resolution Imaging Science Experiment (a-b, d) images of the mantling unit, ESP_016520_1750_RED, ESP_013540_1745_RED, ESP_024023_1755_RED, and (c) digital terrain model of the mantling exposures (orange arrows and white labeled arrow) and the marker band (yellow arrows and white labeled arrows) at 3× vertical exaggeration in SW Mt. Sharp. Blue arrows indicate the uphill direction.

across northern Mt. Sharp of ∼31.8 km with elevations ranging from −4,000 to −1,550 m (Figure S2 in Supporting Information S1), with mapped exposures of lower confidence up to −800 m.

4.2. Composition of the Marker Band and Related Units

CRISM reflectance spectra of the mapped units in this study as well as those of modern aeolian sand in Gale crater were compared across Mt. Sharp (Figures 6–10). Here, we describe both prominent features as well as subtle spectral variations observed. Some regions of the units exhibited neutral spectra, likely due to dust cover. However, our focus is on the spectra that displayed absorptions suitable for comparison in this study.

4.2.1. The Marker Band and Other Layers Confined to Mt. Sharp Stratigraphy

The spectral properties of erosion-resistant layers within the stratigraphy of Mt. Sharp vary with location (Figure 6). In the northwest region of Mt. Sharp, both the high albedo bench-forming strata (Figure 6, spectrum 1) and main marker band package layers are present (Figure 6, spectra 2–4). Spectra obtained from this region consistently exhibit a broad and deep absorption band centered between 1.04 and 1.10 μm, indicating the presence of olivine and/or basaltic glass. The spectrum of the high albedo layer (Figure 6, spectrum 1) remains relatively flat in the 2 μm region until ∼2.4 μm, where it has a blue (i.e., negative) slope toward longer wavelengths. This is consistent with the presence of PHS (Figure 2). There is a possible narrow absorption band centered between 1.9 and 2.0 μm that could be consistent with hydration but is more likely a result of atmospheric CO_2 (e.g., D'Aversa et al., 2022). As there are no detectable broad absorption bands near 2 μm that would indicate the presence of pyroxene or glass, we propose this spectrum dominantly represents a mixture of olivine and PHS. The remaining three spectra in this region correspond to the marker band NW package. Spectrum 2 is from an upper layer, spectrum 3 from the main marker band, and spectrum 4 from a lower layer. Both spectra 2 and 3 both have an apparent 2 μm broad absorption

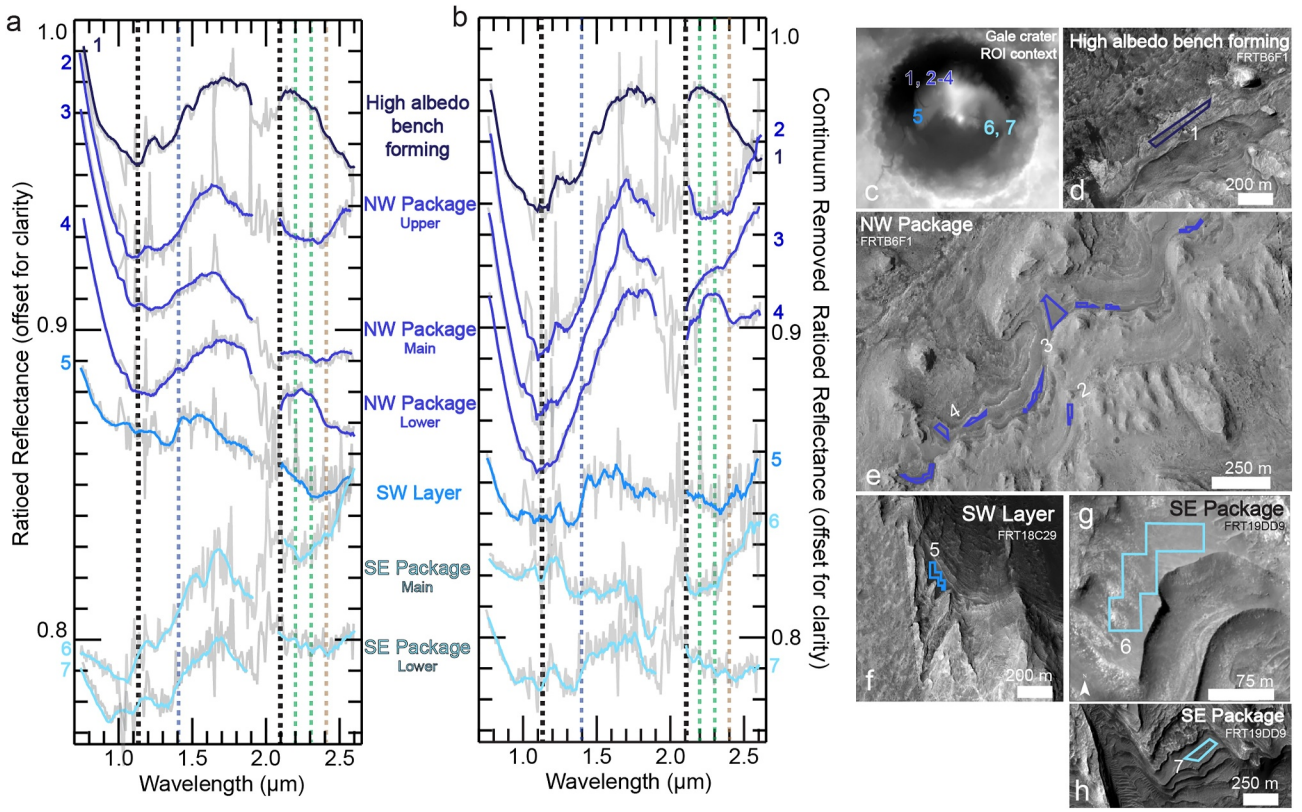

Figure 6. Ratioed reflectance spectra (left) and continuum removed spectra (middle) of bench-forming layers with approximate region of interest locations on High Resolution Imaging Science Experiment images and a context map on a High-Resolution Stereo Camera digital terrain model image (right). Gray spectra represent raw Compact Reconnaissance Imaging Spectrometer for Mars spectra, color spectra represent smoothed and de-spiked spectra. Colors vary based on relative location on Mt. Sharp. Dashed lines on spectral plots correspond to approximate locations of dominant 1 μm absorption for the marker band (black), hydration features at 1.4 μm (blue), Fe-/Mg-/Al-clay absorptions and/or hydrated silica at 2.2 and 2.3 μm (green) and sulfates (tan) at 2.4 μm.

band, which could be attributed to pyroxene and/or glass. However, due to atmospheric CO_2 features in the spectra, the exact wavelength is uncertain (e.g., D'Aversa et al., 2022). Spectrum 4, on the other hand, does not clearly exhibit a broad 2 μm absorption band, but there is a possible narrow absorption at ~2.4 μm that could be due to the presence of monohydrated sulfates (MHS). Overall, olivine and/or glass signatures dominate the northwest layers, potentially mixing with pyroxene and sulfates.

On the western region of Mt. Sharp, only one layer of the marker band is observed, but the spectra of this layer are unreliable for mineral identification (Figure 6, spectrum 5). There are apparent broad and shallow 1 and 2 μm absorption bands, which could be consistent with pyroxene and/or glass, but the data are not clear enough to make a confident determination.

In the SE package, multiple potential marker band layers are observed; two of which, spectra 6 and 7, are shown in Figure 6. Spectrum 7 shares similar characteristics with spectrum 5 from the SW layer, displaying a possible 1 μm absorption band. Spectrum 6 exhibits possible shallow and narrow absorption bands centered at ~1.1, ~1.3, ~1.6 μm which are not consistent with any known relevant minerals and are most likely artifacts. Both spectra 6 and 7 have possible multiple narrow or a singular broad absorption in the 2.2–2.4 μm range which could be attributed to various types of alteration minerals (Fe/Mg/Al-clay minerals, hydrated silica). However, without any other clear spectral features observed, these signatures are not sufficient to confidently identify the composition. Overall, spectra obtained from the marker band exposures outside the NW package may be consistent with a combination of pyroxene, glass, and alteration minerals, but due to limited large exposures and the low CRISM spatial resolution (18 m/pixel), the spectra of marker band exposures across the rest of Mt. Sharp often have more noise, while they are still useful, making them slightly less reliable for composition identification. Because of this, geomorphologic characteristics in addition to the compositional properties are critical for identifying the marker band across Mt. Sharp.

4.2.2. The Mound Skirting Unit

The highest quality spectra of the MSU are obtained from the western side of Mt. Sharp and are depicted in Figure 7. In the northwest region, spectra were acquired from the rover-explored region of the MSU Stimson formation (Figure 7, spectra 1 and 2). These spectra exhibit a broad and deep absorption band centered between 1.08 and 1.10 μm, along with an additional broad and shallow absorption band centered at 2.30 μm and a narrow absorption centered between 2.3 and 2.4 μm. Similar broad spectral features are observed in the southwest region of Mt. Sharp (Figure 7, spectra 4 and 5) along with the northwest exposures of the MSU. However, in the southwest region, the 1 μm band absorption occurs at a slightly shorter wavelength (1.04 μm), while the 2 μm absorption band center is at 2.27 μm. Spectrum 4 has a slightly red (i.e., positive) overall slope. These spectral characteristics of the broad absorption bands are consistent with a combination of olivine and/or glass mixed with high-Ca pyroxene and the narrow absorption in spectra 1 and 2 are consistent with Fe/Mg-clays and/or -sulfates. Spectrum 3 in the MSU displays potential broad and shallow absorption bands in the 1 and 2 μm regions. Although these bands are less

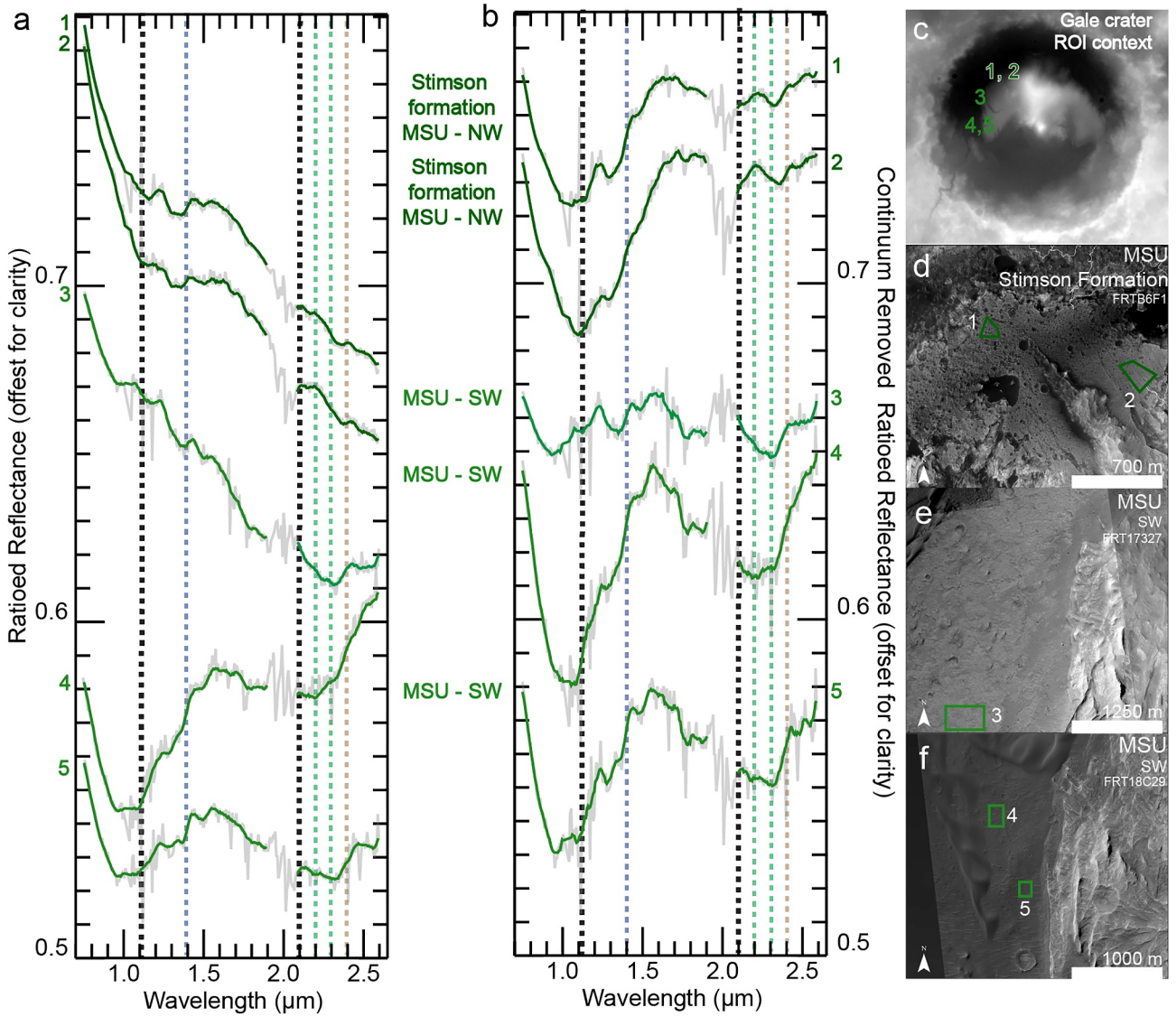

Figure 7. Ratioed reflectance spectra (left) and continuum removed spectra (middle) of mound skirting unit exposures with approximate region of interest locations on High Resolution Imaging Science Experiment images and a context map on a High-Resolution Stereo Camera digital terrain model image (right). Gray spectra represent raw Compact Reconnaissance Imaging Spectrometer for Mars spectra and color spectra represent smoothed and de-spiked spectra. Colors vary based on relative location on Mt. Sharp. Dashed lines on spectral plots correspond to approximate locations of dominant 1 μm absorption for the marker band (Figure 6, spectrum 3, black line), hydration features at 1.4 μm (blue), Fe-/Mg-/Al-clay absorptions and/or hydrated silica at 2.2 and 2.3 μm (green) and sulfates (tan) at 2.4 μm.

distinct, band centers are present at 1.05 and 2.27 μm, which is consistent with high-Ca pyroxene. Spectra 1–3 have a steep blue (i.e., negative) slope that has been previously attributed to aphanitic or microcrystalline basalts and is consistent with a primarily mafic mineral composition (e.g., Henderson et al., 2021; Scudder et al., 2021). Overall, spectral signatures from the MSU exhibit similarities to the exposures of the NW marker band package. These similarities suggest a composition consisting of a mixture of olivine and/or glass along with the presence of high-Ca pyroxene, with the addition of possible Fe/Mg-clay and/or -sulfates in the MSU.

4.2.3. The Mantling Unit

In the northwest region of Mt. Sharp, the mantling unit spectra (Figure 8, spectrum 1) exhibit two broad and shallow absorption bands centered at 1.02 and 2.23 μm consistent with the presence of high-Ca pyroxene. Moving to the southwest side of Mt. Sharp (Figure 8, spectra 2 and 3), spectrum 2 exhibits a broad and deep absorption band centered at 1.04 μm, along with a broad and shallow absorption band centered at 2.27 μm consistent with a mixture of olivine and/or glass as well as high-Ca pyroxene. The mantling unit near the marker band on southwest Mt. Sharp (Figure 8, spectrum 3) displays broad and shallow absorption bands centered at 1.02 and 2.20 μm, consistent with high-Ca pyroxene. It is possible that some of the pyroxene spectral signatures at lower elevations (Figure 8, spectrum 2) correspond to sand eroded off this unit.

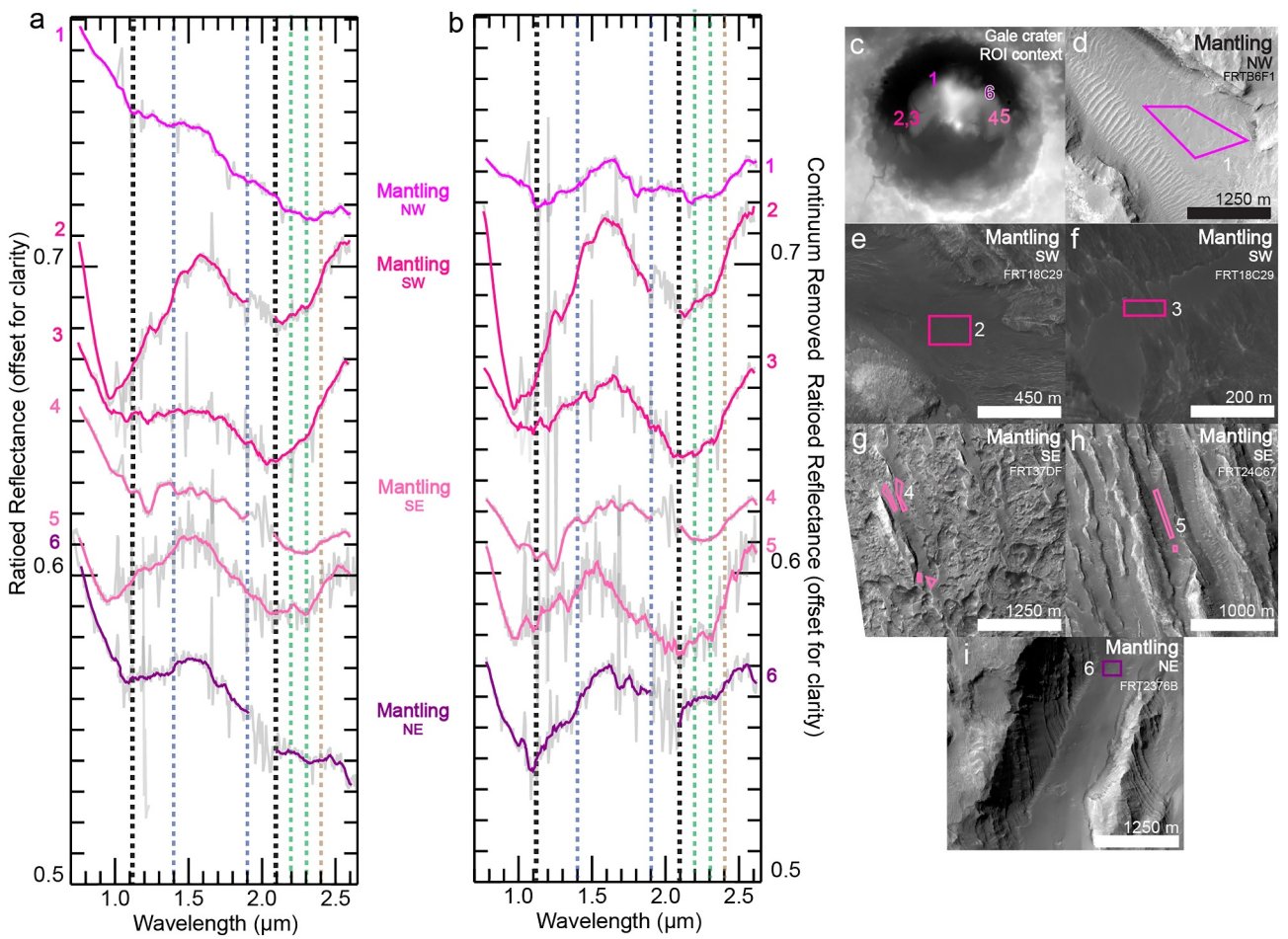

Figure 8. Ratioed reflectance spectra (left) and continuum removed spectra (middle) of mantling unit exposures with approximate region of interest locations on High Resolution Imaging Science Experiment images and a context map on a High-Resolution Stereo Camera digital terrain model image (right). Gray spectra represent raw Compact Reconnaissance Imaging Spectrometer for Mars spectra and color spectra represent smoothed and de-spiked spectra. Colors vary based on relative location on Mt. Sharp. Dashed lines on spectral plots correspond to approximate locations of dominant 1 μm absorption for the marker band (Figure 6, spectrum 3, black line), hydration features at 1.4 μm (blue), Fe-/Mg-/Al-clay absorptions and/or hydrated silica at 2.2 and 2.3 μm (green) and sulfates (tan) at 2.4 μm.

In southeast Mt. Sharp, spectra exhibit two broad absorption bands with slightly different band shapes (Figure 8, spectra 4 and 5). Spectrum 4 has a red slope between approximately 1.2 and 1.4 μm, but it still exhibits a broad and shallow absorption band centered at 1.00 μm, along with a possible broad and shallow absorption band centered at 2.24 μm. The identification of the 2 μm absorption band is uncertain due to a combination of noise resulting from atmospheric CO_2 and the shallow depth of the band in this region. Spectrum 5 has two broad and shallow absorption bands centered at 1.04 and 2.27 μm consistent with high-Ca pyroxene.

In the northeastern region of Mt. Sharp (Figure 8, spectrum 6), the mantling unit exhibits two broad absorptions. One absorption band is deep and centered at 1.02 μm, while the other is broad and shallow, centered at 2.30 μm. This is consistent with a mixture of olivine and/or glass and high-Ca pyroxene. Overall, the mantling unit is primarily composed of unaltered mafic minerals, with high-Ca pyroxene dominating and minor contributions of olivine.

4.2.4. Modern Aeolian Sand

Sand found throughout the Gale crater is hypothesized to originate from various sources, including Mt. Sharp erosion and sand from beyond Gale's rim (Bedford et al., 2020; Cousin et al., 2017; Lapôtre & Rampe, 2018;

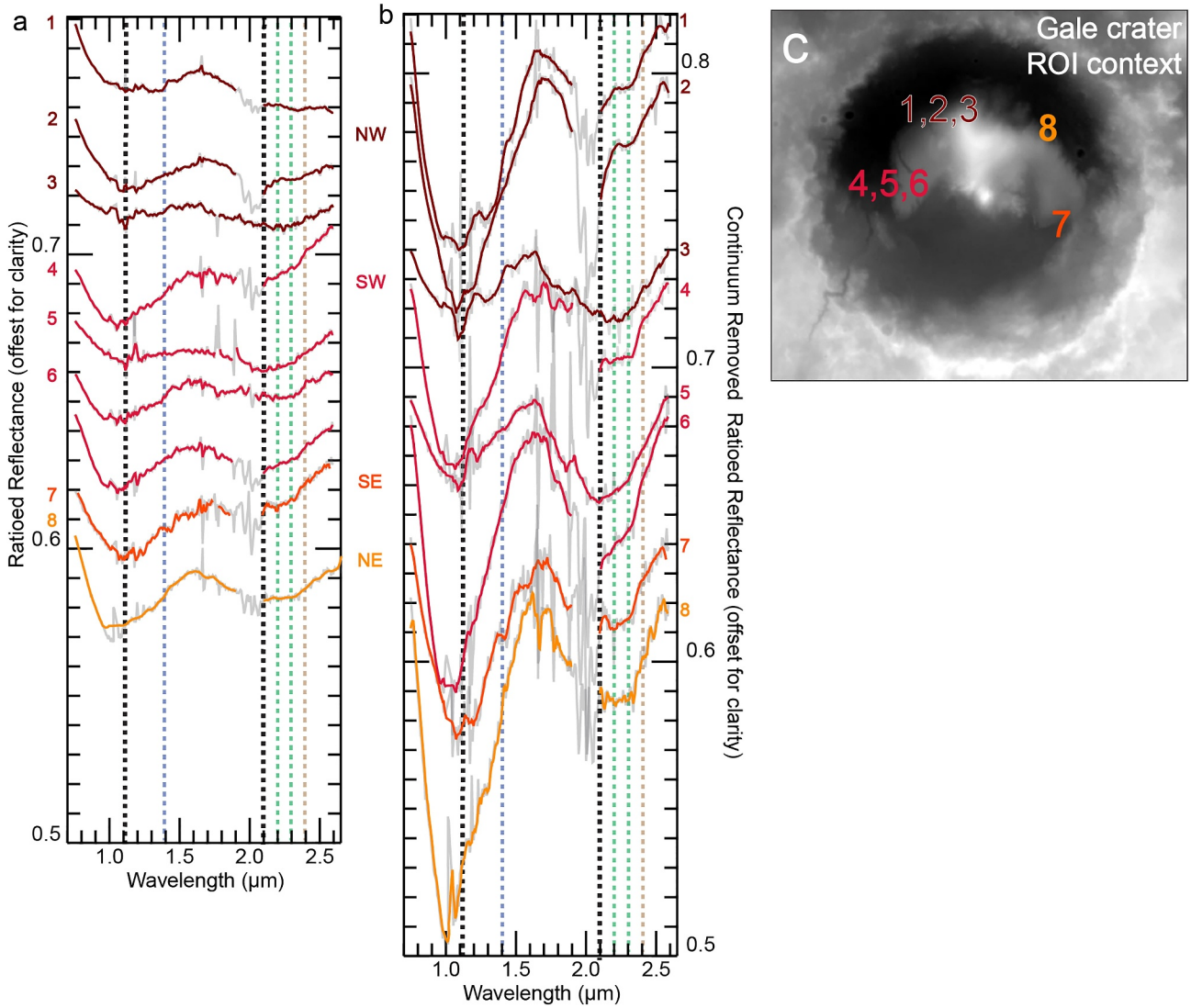

Figure 9. Ratioed reflectance spectra (left) and continuum removed spectra (middle) of active sand. Gray spectra represent raw Compact Reconnaissance Imaging Spectrometer for Mars spectra and color spectra represent smoothed and de-spiked spectra. Colors vary based on relative location on Mt. Sharp. Dashed lines on spectral plots correspond to approximate locations of dominant 1 μm absorption for the marker band (Figure 6, spectrum 3, black line), hydration features at 1.4 μm (blue), Fe-/Mg-/Al-clay absorptions and/or hydrated silica at 2.2 and 2.3 μm (green) and sulfates (tan) at 2.4 μm.

Lapôtre et al., 2017; O'Connell-Cooper et al., 2018). As sand is not a lithified, erosion-resistant unit, we do not discuss morphology or map the extent of active sand deposits. Here we compare the spectral features of the sand to the erosion-resistant units mapped in this study as they are potential sand sources (Figure 9).

Across Mt. Sharp, the sand spectra are dominated by a broad and deep, occasionally asymmetrical absorption band centered between 1.00 and 1.11 μm, along with a broad and shallow absorption band centered between 2.07 and 2.30 μm. These spectral features are consistent with a combination of olivine and/or glass mixed with high-Ca pyroxene. In some sand spectra from the northwest region of Mt. Sharp (Figure 9, spectrum 3) and the western region of Mt. Sharp (Figure 9, spectrum 5), the 1 μm absorption bands are not as deep, suggesting a greater high-Ca pyroxene abundance. This is consistent with previous orbital studies of sand in Gale crater (e.g., Bennett et al., 2018; Moreland et al., 2022) and in situ analyses from the Chemistry and Mineralogy (CheMin) X-ray diffraction instrument (Blake et al., 2012) on board *Curiosity* (Rampe et al., 2018). Overall, the spectral characteristics of the sand most closely resemble the mantling unit exposures across Mt. Sharp, the western exposures of the MSU, and the NW marker band package which are also consistent with a combination of olivine and/or glass mixed with pyroxene, and some resemblance to the high albedo layer, which has olivine but no indication of any pyroxene.

4.2.5. Spectral Parameters

The spectral parameters shown in Figure 10 help to highlight subtle compositional trends based on the absorption band shape, center, and area for the units in this study. Units have spectral features that correspond more closely to their geographic location rather than their specific unit types. This supports a similar composition across these different morphologies with the main source of variability attributed to relative olivine and high-Ca pyroxene content.

In northwestern Mt. Sharp (darkest symbol), the spectra are overall more olivine-rich, while spectra from the southwest (second darkest symbol) have a greater contribution from high-Ca pyroxene, and spectra from the southeast (second lightest symbol) and northeast (lightest symbol) have more variable compositions between olivine and high-Ca pyroxene. This is most evident with the 1 μm band center (Figures 10a and 10c). Band areas (Figure 10b) differentiate the mantling unit (stars) and southern marker band (triangles) exposures from the majority of the MSU (squares) and northwest marker band exposures where the former is more pyroxene rich.

Sand spectra (circles) exhibit a similar trend by grouping together with respect to location, while still having compositions that are dominated by high-Ca pyroxene and olivine. Additionally, the sand spectra plot near all of the different units, with the most distinct trend in the 1 μm band area relative to the 2 μm band area (Figure 10b). In this plot, the sand spectra more closely resemble the MSU but still have spectral similarities to the marker band and mantling units. This observation does align with the fact that the MSU is a confirmed aeolian unit, as are the active sands.

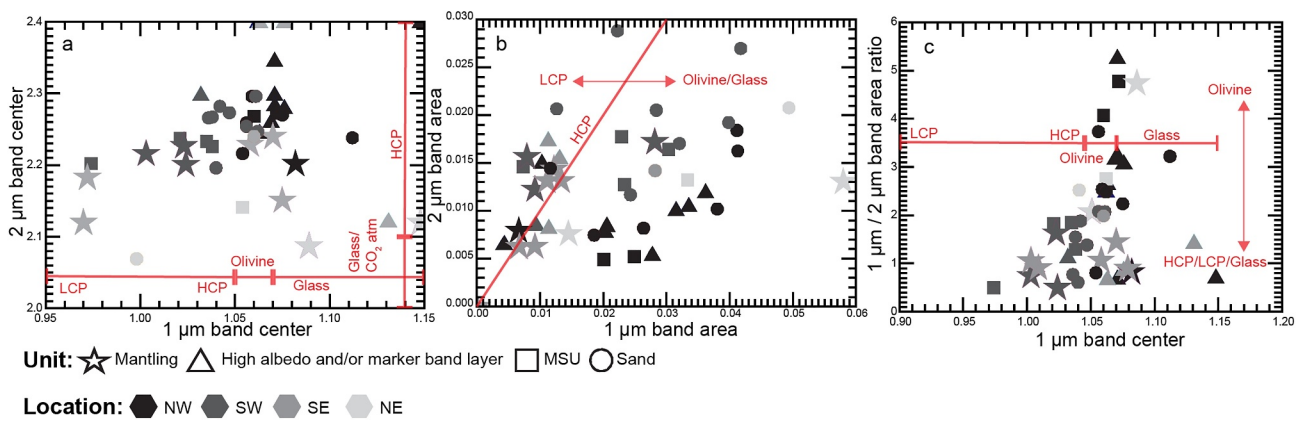

Figure 10. Spectral parameters of fourth order polynomial fit spectra (Figure S1 in Supporting Information S1) used in this study to differentiate trends between mafic minerals. (a) 1 μm band center versus 2 μm band center, (b) 1 μm band area versus 2 μm band area, and (c) 1 μm band center versus 1/2 μm band area ratio. Red lines and arrows represent expected approximate locations for labeled composition based on Horgan et al. (2014). Some points are missing from the 1 μm band center versus 1 μm band asymmetry plot as they plot with very high asymmetry values outside the region shown here and relevant trends could not be observed when shown.

5. Discussion

5.1. Origin of the Marker Band From Orbital and In Situ Analyses

The typical framework for Mars exploration is to use orbital analyses as a guide for surface exploration, but upon in situ investigation, we have often found that the geologic history is much more complicated and can lead to a different interpretation from that originally proposed from orbital analyses (e.g., Edgett & Sarkar, 2021; Fedo et al., 2022). This work explores whether in situ knowledge can be extended to an orbital scale and applied to units that have similar orbital properties to those explored at the surface as a guide to future orbital interpretation. The methodology was tested through the comparison of two units that have been studied from orbit and in situ (the MSU and marker band) to one that has only been explored from orbit (mantling unit).

Previous orbital analyses of the marker band have proposed a single event that deposited the layer across all of Mt. Sharp (e.g., Weitz et al., 2022). We have instead divided this proposed singular layer into multiple packages of marker bands based on their location on Mt. Sharp, which may or may not be laterally equivalent to the main NW marker band explored by *Curiosity*, similar to the relationships proposed in Sheppard et al. (2021). Each package has a different number of potential additional layers, which, if they are laterally equivalent to the marker band, suggests regional variability in the process that formed them. The NW package has 2–3 layers, the SW layer is a single layer, and the SE package has up to four layers. Although all layers are visually similar, their compositions vary at their respective locations. The NW package layers, closest to MSL, are dominated by olivine with some contributions from sulfates, while the marker band exposures in other areas across Mt. Sharp are either more pyroxene rich or their spectra are too noisy to confidently identify the composition. The compositional variability could be caused by localized differences in sediment sources or transport processes. Alternatively, we cannot rule out that this variability is due to contamination by modern sand whose spectral signatures are mostly dominated by olivine across Mt. Sharp.

From orbit, the properties of the marker band seem most consistent with non-aqueous processes, including aeolian, volcanism, and impacts (e.g., Edgett & Sarkar, 2021; Malin & Edgett, 2000; Milliken et al., 2010; Sheppard et al., 2021; Weitz et al., 2022). The lower albedo and mafic spectral properties of the marker band compared to the surrounding higher albedo lacustrine sediments dominated by secondary minerals initially suggest a distinct non-aqueous origin for the marker band based on orbital data. We find that impacts are the least likely of the three due to the repetitive nature of multiple layer exposures. The inferred mafic composition could be consistent with either aeolian sands that were at one point sourced from volcanic rocks prior to erosion and transport or a volcanic ash deposit. Constraining between these two any further would require a closer perspective to see the sedimentary structures present in the bedrock. Aeolian deposits can preserve features such as cross-bedding that represent a migrating surface and can be used to help differentiate them from a volcanic ash deposit, which can generate both thinly and massively bedded deposits (e.g., Wohletz & Sheridan, 1983).

Preliminary results from in situ exploration of the marker band indicate an aqueous environment that was not apparent through orbital analyses alone. Lower strata in the marker band contain symmetrical ripples consistent with an ancient shallow-water, possibly lacustrine, depositional environment that transitions to upper rhythmic laminated strata consistent with a deeper lacustrine depositional environment (Dietrich et al., 2023; Gupta et al., 2023; Parker et al., 2023; Rampe et al., 2023; Roberts et al., 2023; Weitz et al., 2023). Although the environment predicted was unexpected, the compositionally distinct nature of the marker band relative to surrounding units in situ is consistent with orbital analyses. ChemCam, the laser induced breakdown spectrometer in the instrument suite of MSL (Wiens et al., 2012), has found that the marker band has a significantly higher FeO_T content compared to underlying and overlying units, increasing from ∼17.5 to 27 wt.%, and that CaO in bedrock increases compared to the underlying unit (Gasda et al., 2023). The Alpha Particle X-ray Spectrometer in the MSL instrument suite (Campbell et al., 2012; Gellert et al., 2009) has also found the marker band to be consistent with a basaltic composition (Thompson et al., 2023). Additionally, surface images show that the marker band is an erosion-resistant unit relative to the surrounding strata (e.g., Gupta et al., 2023; Roberts et al., 2023; Weitz et al., 2023). It remains unclear why this lacustrine unit observed in the marker band has distinct physical and spectral properties relative to the recessive mudstone and siltstone lacustrine layers that have been previously explored by *Curiosity* in the Murray formation (Grotzinger et al., 2015).

With the in situ knowledge of a lacustrine environment for the marker band, our understanding and resulting hypotheses from orbital observations in this study were able to be re-framed from a new perspective. One

possibility is that the marker band layers represent grain size variability in a lake, where coarser-grained shoreline wave ripples could be more erosion-resistant (i.e., marker band) compared to the previously explored horizontal, fine-grained lacustrine strata that are more representative of the middle of a lake (e.g., Grotzinger et al., 2015). But the distinct chemistry from in situ results compared to previously explored lacustrine units makes this less likely. We hypothesize that the sediment source is distinct relative to the rest of the Murray formation strata and the previously preferred depositional processes from orbital analyses of aeolian or volcanic ash are still plausible in this scenario. Our preferred hypothesis is that mafic aeolian sand (deposited during a dry period) or volcanic ash (deposited during a dry period, into the watershed, or into the lake itself) was deposited into Gale crater, but prior to burial and lithification the region returned to (or stayed as) a lacustrine environment, leaving the wave-ripple structure that we see in situ. The multiple layers in different marker band packages could be a result of fluctuating water levels or intermittent processes such as volcanic eruptions. These early water-sediment interactions could have resulted in the physical properties we see in the marker band layers while still being consistent with a dominantly mafic composition for the sediment source.

5.2. Origin of the MSU From Orbital and In Situ Analyses

Visually and texturally from orbit, the MSU is distinct from the marker band although both are dominated by mafic mineral spectral signatures. Both the albedo of the MSU, which is higher on average than that of the marker band, and its resistance to erosion are more variable, whereas the marker band has consistently low albedo and high resistance to erosion. Compositional similarities with different morphologies between the MSU and the marker band could be a result of a similar sediment source, such as regional sands, that were exposed to different local depositional or diagenetic environments.

The previously proposed depositional environment from orbital analyses by R. Anderson and Bell (2010) for the MSU was aeolian but was still discussed in the literature with some uncertainty prior to ground exploration. However, in situ analyses of the MSU through the Stimson formation of the Siccar Point group did confirm that the MSU along the traverse between sols 987–3,700 is an aeolian unit (e.g., Banham et al., 2018, 2021, 2022, 2023; Bedford et al., 2020). Lithified, erosion-resistant aeolian units are important to understand in the context of the marker band as aeolian processes were one of the dominant hypotheses for marker band depositional processes prior to in situ exploration (Milliken et al., 2010; Rapin et al., 2021; Weitz et al., 2022). The Greenheugh pediment, a particularly erosion-resistant exposure of the MSU, was investigated at a rover scale and has dark- and light-toned veins, consistent with interactions with diagenetic fluids (e.g., Gasda et al., 2022; Rudolph et al., 2022). The Naukluft and Emerson plateaus of the MSU also appear to be erosion resistant, although not quite to the same extent as the Greenheugh pediment. In situ analyses of these plateaus show alteration halos, light-toned veins, and concretions, which are hypothesized to be a result of groundwater interactions (Bedford et al., 2020; Frydenvang et al., 2017; Sun et al., 2019; Yen et al., 2017). The MSU records a dry environment that lacks evidence for surface water contemporaneous with deposition (e.g., the absence of damp interdune deposits; Banham et al., 2018), but it does record evidence of later diagenesis and ground water expressed as soft sediment deformation in some areas that predates lithification, and water escape structures penecontemporaneous with lithification (Banham et al., 2023; Dietrich et al., 2022). From the context of orbital studies, we propose that units that have visual similarities to the MSU rather than the marker band would have had the most exposure to water-rock interactions during and/or after burial and lithification rather than in the primary depositional environment.

5.3. Origins of the Mantling Unit

Our results indicate that the mantling unit could have formed through similar sediment sources and aqueous processes as the marker band. We find that the mantling unit is texturally more similar to the marker band layers than the MSU, although all three units are dominated by mafic mineral or neutral spectral signatures. Both the marker band and mantling unit have a consistently low-albedo, relatively smooth, and erosion resistant surface relative to their surroundings compared to the variable visual properties of the MSU. Given the unique textural expression of the marker band on Mt. Sharp, we hypothesize that the textural similarity in the mantling unit is representative of exposure to and relative timing of similar environments, both during deposition and diagenesis. As mentioned previously, early results from the marker band suggest a lacustrine environment, and if the mantling unit formed in the same environment, this supports existing models for relatively late-stage water activity in Gale crater (e.g., Palucis et al., 2016) as shown through the cross-cutting of the mantling unit over existing Mt. Sharp strata.

The specific sediment source(s) for the units analyzed here are not known, but the compositional similarities suggest a similar, if not the same, source. We hypothesize that these units have a similar sediment source that is distinct from other Mt. Sharp strata that these sediments were transported into Gale crater through an unknown mechanism (e.g., aeolian, fluvial, volcanic airfall), and their present-day morphologic expression is a result of the timing of water-rock/sediment interactions (see Section 5.4).

5.4. Implications for Aqueous History of Gale Crater

Previous in situ analyses of the MSU and early results from the marker band show that they represent different environments (aeolian vs. lacustrine; e.g., Banham et al., 2018; Bedford et al., 2020; Fraeman et al., 2016; Gupta et al., 2023; Parker et al., 2023; Rampe et al., 2023; Roberts et al., 2023; Weitz et al., 2023). We aimed to constrain whether orbital analyses are adequate to differentiate between these environments or if in situ analyses are required to constrain the depositional environment of the mantling unit. We hypothesize that they can be differentiated but only with the informed in situ knowledge that we have now through MSL. We propose that the sediments for all units in this study were brought into Gale crater through aeolian transport (e.g., Thomson et al., 2011), possibly during a dry period, and that the duration of that dry period before transitioning into a wet period had an impact on their modern-day morphologies. We favor aeolian transport as the MSU is an aeolian unit, but again we cannot truly constrain that deposition mechanism. Here we attempt to constrain water-rock and water-sediment interactions recorded by these units and their environmental implications.

The MSU sediments were deposited during a predominantly dry period and were not exposed to extensive water-rock interactions until burial, lithification, and later diagenetic activity (Bedford et al., 2020; Frydenvang et al., 2017; Gasda et al., 2022; Rudolph et al., 2022; Sun et al., 2019; Yen et al., 2017). Spatially varying diagenesis in the MSU was likely caused by variations in porosity and permeability, which regulated groundwater flow and led to variations in albedo and erosional resistance in different exposures. For example, the Greenheugh pediment was exposed to diagenetic fluids for a relatively long period of time because the low permeability of the clay-mineral rich unit led to enhanced alteration near the contact (e.g., Rudolph et al., 2022) and is hypothesized to be a more erosion-resistant part of the MSU possibly as a result of post-landslide burial lithification (R. Anderson & Bell, 2010). The degree of diagenesis was likely a result of local processes for the MSU across Mt. Sharp. We cannot rule out that the MSU has no relation to the marker band layers and mantling unit, and although similar in composition, the orbital spectral characteristics could be a result of modern-day surface sediment transport around the MSU and deposited on top of the MSU bedrock.

We favor the hypothesis that the sediments of the marker band layers were deposited during a dry period but were reworked in a lacustrine environment prior to burial. If that is the case, the multiple marker band layers represent multiple wet-dry fluctuations (e.g., Rapin et al., 2023). This reconciles the wave-ripple morphology of the marker band with a composition that is similar to aeolian units (i.e., MSU). The early exposure to water may also result in a strong cementing process due to prolonged water exposure that allows for the erosion-resistivity that we see in the marker band and in the mantling unit (e.g., Park, 2010).

Because compositions inferred from orbital spectroscopy are similar between the MSU and the marker band, we suggest that morphologic analysis is the best orbital technique to differentiate between the two units and the environments that they represent. For this reason, we propose that the mantling unit is more similar to the marker band rather than to the MSU. If that is the case, the sediments of the mantling unit were exposed to water prior to lithification, either through deposition into an aqueous environment or not long after deposition, and then subsequently buried, lithified, and exposed at the surface to form the morphology we see today. Given the draping nature of the mantling unit, we find it more likely that the depositional process and sediment source for the mantling unit in this scenario was not aqueous, but rather could represent an airfall or aeolian deposition to drape the existing Mt. Sharp strata.

While we suggest that the mantling unit is more closely related to the marker band, the source of water-sediment interactions need not be the same for the two units. For the marker band, the wave-ripple morphologies suggest sediment reworking in a lacustrine environment, but there are other possibilities to explore for the mantling unit (e.g., early groundwater interactions, or water derived from snowmelt; Kite et al., 2013; Koeppel et al., 2022). The disconnected portions of the mantling unit along eastern Mt. Sharp (Figure 5a) has a morphology that may be indicative of subsurface groundwater flow (e.g., Bernatek-Jakiel & Poesen, 2018; Scuderi, Gallegos, et al., 2019; Scuderi, Nagle-McNaughton, et al., 2019). Alternatively, if the mantling unit corresponds to a late-stage

lacustrine environment, it may correspond to near-shore environments during the Pancake delta lake stand, as mapped by Palucis et al. (2016). The elevation of the proposed lake level is near the top of the valleys that the mantling units slope down into (−3,280 m). This lake is proposed to have been present after erosion of the Mt. Sharp strata into the topography that we see today (Palucis et al., 2016). We also cannot rule out that the mantling unit represents another exposure of the MSU but one that has been less diagenetically altered, whether that be a result of the higher elevations or a later time of deposition so the mantling unit would have had less time to be altered (e.g., Chojnacki et al., 2020).

While the compositions of each unit are dominated by mafic minerals, there are spectral features consistent with alteration present across the three units, primarily those associated with Fe/Mg/Al-clays, hydrated silica, and/or sulfates (notably in the 2.2–2.5 μm range). But the exact location and shape of these features are inconsistent across both units and locations in Mt. Sharp. We hypothesize that this is a result of spatial variation in alteration rather than differences in sediment source. Possible local alteration process could include weathering to clay minerals and/or evaporation of brines to form sulfates.

The relative timing between the deposition of the MSU and mantling unit is unconstrained as there are no locations in which one unit clearly crosscuts the other, but they were both deposited after Mt. Sharp eroded to its current topographic expression, and thus long after the marker band layers, which are confined within the stratigraphy of Mt. Sharp. If the relationship could be constrained, there are important implications for dry periods in Gale crater, as represented by the MSU, and wet periods in Gale crater, as represented by the mantling unit. There may be some significance to the fact that the MSU is primarily observed at the base of Mt. Sharp while the mantling unit is observed on top of Mt. Sharp.

5.5. Interpreting Orbital Data in Sedimentary Settings on Mars

We have shown that an improved understanding of geologic history using orbital data can be gained with new knowledge from in situ exploration in regions that have not yet or will not be explored from the ground. The results from this study could indicate that water-rock interactions that are readily observed in situ should be included as hypotheses for sedimentary units that have erosion resistant properties similar to the marker band from orbit. This information can inform future work on landing site selection and orbital data analysis.

6. Conclusion

In this study, we compared orbital-scale morphology and spectral observations across multiple distinct units. Combined with previous interpretations through in situ outcrop analysis, we have gained a better understanding of the history of lacustrine and aeolian environments in the stratigraphy of Mt. Sharp. Spectral features of these units, while dominated by overall mafic sediments, vary with location along Mt. Sharp rather than strictly varying by specific morphologic unit. We hypothesize that morphology indicates that similar processes leave behind similar bedrock expressions that are observable from orbit regardless of minor compositional variability.

The mantling unit is most similar in both appearance and composition to the marker band layers, a lacustrine unit, rather than the MSU, an aeolian unit, suggesting that a similar aqueous environment to the marker band layer also occurred later in time to form the mantling unit. This repeating process is also supported by the exposures of multiple marker band-like layers within the stratigraphy of Mt. Sharp, although these were closer in time to the marker band than the mantling unit. If true, these results suggest that both surface and subsurface water activity continued within the Gale crater long after the erosion of Mt. Sharp.

Our results support the hypothesis that the marker band packages, mantling unit, and MSU had a similar sediment source but experienced aqueous alteration at different times: early ubiquitous cementation in a surface aqueous environment in the marker band and mantling unit versus patchy late diagenesis in the MSU. These early water-sediment interactions can lead to distinct orbital morphologies like those observed in the marker band packages and mantling unit. If units of a similar morphologic expression are studied on Mars from orbit, an aqueous depositional environment should be considered.

Data Availability Statement

The data in this publication are from the CRISM, HiRISE, and CTX instruments on Mars Reconnaissance Orbiter and the HRSC instrument on the Mars Express orbiter. All image data presented here from CRISM (S. Murchie, 2006; F. Seelos, 2016), HiRISE (McEwen, 2007a, 2007b), and CTX (Malin, 2007) are available through the Planetary Data System Imaging Node (https://pds-imaging.jpl.nasa.gov/volumes/mro.html) and Geosciences Node (https://pds-geosciences.wustl.edu/missions/mro/default.htm). All image data presented here from HRSC (Neukum et al., 2004) are available through the United States Geological Society Astrogeology Planetary Data System Cartography and Imaging Sciences Node Annex (https://astrogeology.usgs.gov/search/map/mars_mgs_mola_mex_hrsc_blended_dem_global_200m). ArcGIS shapefiles and CRISM ROIs and derived data used in this paper are available (Rudolph, 2024).

Acknowledgments
We would like to thank the Mars Science Laboratory science team for helpful discussion, insight, and input. We also thank the U.S. Geological Survey Astrogeology Science Center, Tenielle Gaither, Glen Cushing, Paul Geissler, and Kevin Jones for their reviews and helpful comments. Additionally, we would like to thank the anonymous reviewers of this journal for their valuable comments. This material is based upon work supported by the National Science Foundation Graduate Research Fellowship Program under Grant DGE-1842166, the Indiana Space Grant Consortium, and the Amelia Earhart Doctoral Fellowship. Any use of trade, firm, or product names is for descriptive purposes only and does not imply endorsement by the U.S. Government.

References

Adams, J. B. (1968). Lunar and Martian surfaces: Petrologic significance of absorption bands in the near-infrared. *Science*, *159*(3822), 1453–1455. https://doi.org/10.1126/science.159.3822.1453

Adams, J. B. (1974). Visible and near-infrared diffuse reflectance spectra of pyroxenes as applied to remote sensing of solid objects in the solar system. *Journal of Geophysical Research*, *79*(32), 4829–4836. https://doi.org/10.1029/jb079i032p04829

Anderson, R., & Bell, J. (2010). Geologic mapping and characterization of Gale Crater and implications for its potential as a Mars Science Laboratory landing site. *The Mars Journal*, *5*, 76–128. https://doi.org/10.1555/mars.2010.0004

Anderson, R. B., Edgar, L. A., Rubin, D. M., Lewis, K. W., & Newman, C. (2018). Complex bedding geometry in the upper portion of Aeolis Mons, Gale Crater, Mars. *Icarus*, *314*, 246–264. https://doi.org/10.1016/j.icarus.2018.06.009

Banham, S. G., Gupta, S., Rubin, D. M., Bedford, C. C., Edgar, L. A., Bryk, A. B., et al. (2022). Evidence for fluctuating wind in shaping an ancient Martian dune field: The Stimson formation at the Greenheugh pediment, Gale crater. *Journal of Geophysical Research: Planets*, *127*(9), e2021JE007023. https://doi.org/10.1029/2021je007023

Banham, S. G., Gupta, S., Rubin, D. M., Edgett, K. S., Barnes, R., Van Beek, J., et al. (2021). A rock record of complex aeolian bedforms in a Hesperian desert landscape: The Stimson formation as exposed in the Murray buttes, Gale crater, Mars. *Journal of Geophysical Research: Planets*, *126*(4), e2020JE006554. https://doi.org/10.1029/2020je006554

Banham, S. G., Gupta, S., Rubin, D. M., Watkins, J. A., Sumner, D. Y., Edgett, K. S., et al. (2018). Ancient Martian aeolian processes and palaeomorphology reconstructed from the Stimson formation on the lower slope of Aeolis Mons, Gale crater, Mars. *Sedimentology*, *65*(4), 993–1042. https://doi.org/10.1111/sed.12469

Banham, S. G., Roberts, A. L., Gupta, S., Dietrich, W. E., Bryk, A. B., Rubin, D. M., & Vasavada, A. R. (2023). Fluidization structures within the Stimson formation: Evidence for water postdating the exhumation of Aeolis Mons. In *Lunar and planetary science conference* (p. 2103).

Bedford, C. C., Banham, S. G., Bridges, J. C., Forni, O., Cousin, A., Bowden, D., et al. (2022). An insight into ancient aeolian processes and post-Noachian aqueous alteration in Gale Crater, Mars, using ChemCam geochemical data from the Greenheugh capping unit. *Journal of Geophysical Research: Planets*, *127*(9), e2021JE007100. https://doi.org/10.1029/2021JE007100

Bedford, C. C., Schwenzer, S. P., Bridges, J. C., Banham, S., Wiens, R. C., Gasnault, O., et al. (2020). Geochemical variation in the Stimson formation of Gale crater: Provenance, mineral sorting, and a comparison with modern Martian dunes. *Icarus*, *341*, 113622. https://doi.org/10.1016/j.icarus.2020.113622

Bennett, K. A., Hill, J. R., Murray, K. C., Edwards, C. S., Bell, J. F., & Christensen, P. R. (2018). THEMIS-VIS investigations of sand at Gale Crater. *Earth and Space Science*, *5*(8), 352–363. https://doi.org/10.1029/2018EA000380

Bernatek-Jakiel, A., & Poesen, J. (2018). Subsurface erosion by soil piping: Significance and research needs. *Earth-Science Reviews*, *185*, 1107–1128. https://doi.org/10.1016/j.earscirev.2018.08.006

Bibring, J.-P., Combes, M., Langevin, Y., Soufflot, A., Cara, C., Drossart, P., et al. (1989). Results from the ISM experiment. *Nature*, *341*(6243), 591–593. https://doi.org/10.1038/341591a0

Bishop, J. L., Lane, M. D., Dyar, M. D., & Brown, A. J. (2008). Reflectance and emission spectroscopy study of four groups of phyllosilicates: Smectites, kaolinite-serpentines, chlorites and micas. *Clay Minerals*, *43*(1), 35–54. https://doi.org/10.1180/claymin.2008.043.1.03

Bishop, J. L., Pieters, C. M., & Edwards, J. O. (1994). Infrared spectroscopic analyses on the nature of water in Montmorillonite. *Clays and Clay Minerals*, *42*(6), 702–716. https://doi.org/10.1346/CCMN.1994.0420606

Blake, D., Vaniman, D., Achilles, C., Anderson, R., Bish, D., Bristow, T., et al. (2012). Characterization and calibration of the CheMin mineralogical instrument on Mars science laboratory. *Space Science Reviews*, *170*(1–4), 341–399. https://doi.org/10.1007/s11214-012-9905-1

Campbell, J. L., Perrett, G. M., Gellert, R., Andrushenko, S. M., Boyd, N. I., Maxwell, J. A., et al. (2012). Calibration of the Mars science Laboratory alpha particle X-ray spectrometer. *Space Science Reviews*, *170*(1–4), 319–340. https://doi.org/10.1007/s11214-012-9873-5

Chojnacki, M., Fenton, L. K., Weintraub, A. R., Edgar, L. A., Jodhpurkar, M. J., & Edwards, C. S. (2020). Ancient Martian aeolian sand dune deposits recorded in the stratigraphy of Valles Marineris and implications for past climates. *Journal of Geophysical Research: Planets*, *125*(9), e2020JE006510. https://doi.org/10.1029/2020JE006510

Clark, R. N., & Roush, T. L. (1984). Reflectance spectroscopy: Quantitative analysis techniques for remote sensing applications. *Journal of Geophysical Research*, *89*(B7), 6329–6340. https://doi.org/10.1029/JB089iB07p06329

Cloutis, E. A., & Gaffey, M. J. (1991). Spectral-compositional variations in the constituent minerals of mafic and ultramafic assemblages and remote sensing implications. *Earth, Moon, and Planets*, *53*(1), 11–53. https://doi.org/10.1007/bf00116217

Cloutis, E. A., Gaffey, M. J., Smith, D. G. W., & Lambert, R. S. J. (1990). Reflectance spectra of glass-bearing mafic silicate mixtures and spectral deconvolution procedures. *Icarus*, *86*(2), 383–401. https://doi.org/10.1016/0019-1035(90)90226-y

Cloutis, E. A., Hawthorne, F., Mertzman, S., Krenn, K., Craig, M., Marcino, D., et al. (2006). Detection and discrimination of sulfate minerals using reflectance spectroscopy. *Icarus*, *184*(1), 121–157. https://doi.org/10.1016/j.icarus.2006.04.003

Cousin, A., Dehouck, E., Meslin, P., Forni, O., Williams, A. J., Stein, N., et al. (2017). Geochemistry of the Bagnold dune field as observed by ChemCam and comparison with other aeolian deposits at Gale Crater. *Journal of Geophysical Research: Planets*, *122*(10), 2144–2162. https://doi.org/10.1002/2017je005261

D'Aversa, E., Oliva, F., Altieri, F., Sindoni, G., Carrozzo, F. G., Bellucci, G., et al. (2022). Vertical distribution of dust in the Martian atmosphere: OMEGA/MEx limb observations. *Icarus*, *371*, 114702. https://doi.org/10.1016/j.icarus.2021.114702

Dietrich, W. E., Bryk, A. B., Banham, S. G., Rubin, D. M., Thompson, L. M., Caravaca, G., & Williams, R. E. (2022). Climate and diagenetic implications of possible soft sediment deformation of the basal aeolian Stimson sediments in Gale Crater. In *53rd lunar and planetary science conference* (p. 1263).

Dietrich, W. E., Bryk, A. B., Kite, E., Lewis, K. W., Gupta, S., Weitz, C. M., et al. (2023). Implications of the local topography of the marker band contact, Gale Crater. In *54th Lunar and planetary science conference* (p. 2806).

Edgar, L. A., Fedo, C. M., Gupta, S., Banham, S. G., Fraeman, A. A., Grotzinger, J. P., et al. (2020). A lacustrine paleoenvironment recorded at Vera RubinRidge, Gale Crater: Overview of the sedimentology and stratigraphy observed by the Mars science Laboratory curiosity rover. *Journal of Geophysical Research: Planets*, *125*(3), e2019JE006307. https://doi.org/10.1029/2019JE006307

Edgett, K. S., & Sarkar, R. (2021). Recognition of sedimentary rock occurrences in satellite and Aerial images of other worlds—Insights from Mars. *Remote Sensing*, *13*(21), 4296. https://doi.org/10.3390/rs13214296

Fedo, C. M., Bryk, A. B., Edgar, L. A., Bennett, K. A., Fox, V. K., Dietrich, W. E., et al. (2022). Geology and stratigraphic correlation of the Murray and Carolyn shoemaker formations across the glen Torridon region, Gale Crater, Mars. *Journal of Geophysical Research: Planets*, *127*(9), e2022JE007408. https://doi.org/10.1029/2022JE007408

Fergason, R. L., Hare, T. M., & Laura, J. (2018). *HRSC and MOLA blended digital elevation model at 200 m v2. Astrogeology PDS Annex*. U.S. Geological Survey. Retrieved from http://bit.ly/HRSC_MOLA_Blend_v0

Fraeman, A. A., Ehlmann, B. L., Arvidson, R. E., Edwards, C. S., Grotzinger, J. P., Milliken, R. E., et al. (2016). The stratigraphy and evolution of lower Mount Sharp from spectral, morphological, and thermophysical orbital data sets. *Journal of Geophysical Research: Planets*, *121*(9), 1713–1736. https://doi.org/10.1002/2016je005095

Frydenvang, J., Gasda, P. J., Hurowitz, J. A., Grotzinger, J. P., Wiens, R. C., Newsom, H. E., et al. (2017). Diagenetic silica enrichment and late-stage groundwater activity in Gale crater, Mars. *Geophysical Research Letters*, *44*(10), 4716–4724. https://doi.org/10.1002/2017gl073323

Gasda, P. J., Comellas, J., Essunfeld, A., Das, D., Bryk, A. B., Dehouck, E., et al. (2022). Overview of the morphology and chemistry of diagenetic features in the clay-rich glen Torridon unit of Gale Crater, Mars. *Journal of Geophysical Research: Planets*, *127*(12), e2021JE007097. https://doi.org/10.1029/2021je007097

Gasda, P. J., Lanza, N., Rapin, W., Frydenvang, J., Goetz, W., Schwenzer, S. P., et al. (2023). ChemCam observations of the marker band, Gale Crater, Mars. In *54th lunar and planetary science conference* (p. 2389).

Gellert, R., Campbell, J. L., King, P. L., Leshin, L. A., Lugmair, G. W., Spray, J. G., & Yen, A. S. (2009). The alpha-particle-X-ray-spectrometer (APXS) for the Mars science laboratory (MSL) rover mission. In *40th lunar and planetary science conference* (p. 2364).

Grotzinger, J. P., Gupta, S., Malin, M. C., Rubin, D. M., Schieber, J., Siebach, K., et al. (2015). Deposition, exhumation, and paleoclimate of an ancient lake deposit, Gale crater, Mars. *Science*, *350*(6257), aac7575. https://doi.org/10.1126/science.aac7575

Grotzinger, J. P., Joy, C., Vasavada, A. R., Anderson, R. C., Baker, C. J., Barry, R., et al. (2012). Mars science laboratory mission and science investigation. *Space Science Reviews*, *170*(1–4), 5–56. https://doi.org/10.1007/s11214-012-9892-2

Grotzinger, J. P., Sumner, D. Y., Kah, L. C., Stack, K., Gupta, S., Edgar, L., et al. (2014). A habitable fluvio-lacustrine environment at Yellowknife Bay, Gale Crater, Mars. *Science*, *343*, 6169. https://doi.org/10.1126/science.1242777

Gupta, S., Dietrich, W., Lewis, K. W., Kite, E. S., Mondro, C., Schieber, J., et al. (2023). High' but not so dry on Aeolis Mons: Transient lake systems in Hesperian deserts in Gale crater. In *53rd lunar and planetary science conference* (p. 2707).

Gupta, S., Edgar, L., Yingst, R. A., Bryk, A., Caravaca, G., Dietrich, W., et al. (2022). Episodic aqueous conditions punctuated dominantly aeolian deposition within the layered sulphate-bearing unit, Gale crater (Mars). In *Europlanet science Congress. Oral*. https://doi.org/10.5194/epsc2022-963

Henderson, M. J. B., Horgan, B. H. N., Rowe, M. C., Wall, K. T., & Scudder, N. A. (2021). Determining the volcanic eruption style of tephra deposits from infrared spectroscopy. *Earth and Space Science*, *8*(2), e2019EA001013. https://doi.org/10.1029/2019EA001013

Horgan, B. H. N., Anderson, R. B., Dromart, G., Amador, E. S., & Rice, M. S. (2020). The mineral diversity of Jezero crater: Evidence for possible lacustrine carbonates on Mars. *Icarus*, *339*, 113526. https://doi.org/10.1016/j.icarus.2019.113526

Horgan, B. H. N., Cloutis, E. A., Mann, P., & Bell, J. F. (2014). Near-infrared spectra of ferrous mineral mixtures and methods for their identification in planetary surface spectra. *Icarus*, *234*, 132–154. https://doi.org/10.1016/j.icarus.2014.02.031

King, T. V. V., & Ridley, W. I. (1987). Relation of the spectroscopic reflectance of olivine to mineral chemistry and some remote sensing implications. *Journal of Geophysical Research*, *92*(B11), 11457–11469. https://doi.org/10.1029/jb092ib11p11457

Kite, E. S., Halevy, I., Kahre, M. A., Manga, M., & Wolff, M. (2013). Seasonal melting and the formation of sedimentary rocks on Mars. *Icarus*, *223*(1), 181–210. https://doi.org/10.1016/j.icarus.2012.11.034

Kite, E. S., Sneed, J., Mayer, D. P., Lewis, K. W., Michaels, T. I., Hore, A., & Rafkin, S. C. R. (2016). Evolution of major sedimentary mounds on Mars: Buildup via anticompensational stacking modulated by climate change. *Journal of Geophysical Research: Planets*, *121*(11), 2282–2324. https://doi.org/10.1002/2016JE005135

Klima, R. L., Dyar, M. D., & Pieters, C. M. (2011). Near-infrared spectra of clinopyroxenes: Effects of calcium content and crystal structure. *Meteoritics & Planetary Sciences*, *46*(3), 379–395. https://doi.org/10.1111/j.1945-5100.2010.01158.x

Klima, R. L., Pieters, C. M., & Dyar, M. D. (2007). Spectroscopy of synthetic Mg-Fe pyroxenes I: Spin-allowed and spin-forbidden crystal field bands in the visible and near-infrared. *Meteoritics & Planetary Sciences*, *42*(2), 235–253. https://doi.org/10.1111/j.1945-5100.2007.tb00230.x

Koeppel, A. H., Edwards, C. S., Annex, A. M., Lewis, K. W., & Carrillo, G. J. (2022). A fragile record of fleeting water on Mars. *Geology*, *50*(2), 152–157. https://doi.org/10.1130/G49285.1

Kokaly, R. F., Clark, R. N., Swayze, G. A., Livo, K. E., Hoefen, T. M., Pearson, N. C., et al. (2017). USGS spectral Library version 7: U.S. Geological Survey data series, 1035 (p. 61). https://doi.org/10.3133/ds1035

Kronyak, R. E., Kah, L. C., Edgett, K. S., VanBommel, S. J., Thompson, L. M., Wiens, R. C., et al. (2019). Mineral-filled fractures as indicators of multigenerational fluid flow in the Pahrump Hills member of the Murray formation, Gale Crater, Mars. *Earth and Space Science*, *6*(2), 238–265. https://doi.org/10.1029/2018EA000482

Langevin, Y., Poulet, F., Bibring, J.-P., & Gondet, B. (2005). Sulfates in the north polar region of Mars detected by OMEGA/Mars express. *Science*, *307*(5715), 1584–1586. https://doi.org/10.1126/science.1109091

Lapôtre, M. G. A., Ehlmann, B. L., Minson, S. E., Arvidson, R. E., Ayoub, F., Fraeman, A. A., et al. (2017). Compositional variations in sands of the Bagnold Dunes, Gale crater, Mars, from visible-shortwave infrared spectroscopy and comparison with ground truth from the Curiosity rover. *Journal of Geophysical Research: Planets*, *122*(12), 2489–2509. https://doi.org/10.1002/2016je005133

Lapôtre, M. G. A., & Rampe, E. B. (2018). Curiosity's investigation of the Bagnold dunes, Gale Crater: Overview of the two-phase Scientific Campaign and introduction to the special collection. *Geophysical Research Letters*, *45*(19), 10200–10210. https://doi.org/10.1029/2018gl079032

Malin, M. C. (2007). *MRO context camera experiment data record level 0 V1.0, MRO-M-CTX-2-EDR-L0-V1.0*. NASA Planetary Data System. https://doi.org/10.17189/1520266
Malin, M. C., Bell, J. F., Cantor, B. A., Caplinger, M. A., Calvin, W. M., Clancy, R. T., et al. (2007). Context camera investigation on board the Mars Reconnaissance orbiter. *Journal of Geophysical Research*, *112*(E5), E05S04. https://doi.org/10.1029/2006je002808
Malin, M. C., & Edgett, K. S. (2000). Sedimentary rocks of early Mars. *Science*, *290*(5498), 1927–1937. https://doi.org/10.1126/science.290.5498.1927
McEwen, A. S. (2007a). *Mars reconnaissance orbiter high resolution imaging science experiment, experiment data record, MRO-M-HIRISE-2-EDR-V1.0*. NASA Planetary Data System. https://doi.org/10.17189/1520179
McEwen, A. S. (2007b). *Mars reconnaissance orbiter high resolution imaging science experiment, reduced data record, MRO-M-HIRISE-3-RDR-V1.1*. NASA Planetary Data System. https://doi.org/10.17189/1520303
McEwen, A. S., Eliason, E. M., Bergstrom, J. W., Bridges, N. T., Hansen, C. J., Delamere, W. A., et al. (2007). Mars reconnaissance orbiter's high resolution imaging science experiment (HiRISE). *Journal of Geophysical Research: Planets*, *112*(E5), E05S02. https://doi.org/10.1029/2005je002605
McGuire, P. C., Bishop, J. L., Brown, A. J., Fraeman, A. A., Marzo, G. A., Morgan, M. F., et al. (2009). An improvement to the volcano-scan algorithm for atmospheric correction of CRISM and OMEGA spectral data. *Planetary and Space Science*, *57*(7), 809–815. https://doi.org/10.1016/j.pss.2009.03.007
Milliken, R. E., Ewing, R. C., Fischer, W. W., & Hurowitz, J. (2014). Wind-blown sandstones cemented by sulfate and clay minerals in Gale Crater, Mars. *Geophysical Research Letters*, *41*(4), 1149–1154. https://doi.org/10.1002/2013GL059097
Milliken, R. E., Grotzinger, J. P., & Thomson, B. J. (2010). Paleoclimate of Mars as captured by the stratigraphic record in Gale Crater. *Geophysical Research Letters*, *37*(4), L04201. https://doi.org/10.1029/2009gl041870
Moreland, E. L., Arvidson, R. E., Morris, R. V., Condus, T., Hughes, M. N., Weitz, C. M., & VanBommel, S. J. (2022). Orbital and in situ investigation of the Bagnold dunes and sands of Forvie, Gale Crater, Mars. *Journal of Geophysical Research: Planets*, *127*(11), e2022JE007436. https://doi.org/10.1029/2022JE007436
Murchie, S. (2006). MRO CRISM targeted Reduced data record V1.0 [Dataset]. *NASA Planetary Data System*. https://doi.org/10.17189/1519450
Murchie, S., Arvidson, R., Bedini, P., Beisser, K., Bibring, J.-P., Bishop, J., et al. (2007). Compact reconnaissance imaging spectrometer for Mars (CRISM) on Mars reconnaissance orbiter (MRO). *Journal of Geophysical Research*, *112*(E5), E05S03. https://doi.org/10.1029/2006je002682
Murchie, S. L., Seelos, F. P., Hash, C. D., Humm, D. C., Malaret, E., McGovern, J. A., et al. (2009). Compact reconnaissance imaging spectrometer for Mars investigation and data set from the Mars reconnaissance Orbiter's primary science phase. *Journal of Geophysical Research*, *114*(E2), E05S03. https://doi.org/10.1029/2009je003344
Neukum, G., Jaumann, R., & the HRSC Co-Investigator and Experiment Team. (2004). HRSC: The high resolution stereo camera of Mars Express. In A. Wilson (Ed.), *Mars express: The scientific payload. Wilson, scientific coordination: Agustin Chicarro. ESA SP-1240* (pp. 17–35). ESA Publications Division.
O'Connell-Cooper, C. D., Thompson, L. M., Spray, J. G., Berger, J. A., VanBommel, S. J., Gellert, R., et al. (2018). Chemical diversity of sands within the linear and Barchan dunes of the Bagnold dunes, Gale Crater, as revealed by APXS Onboard curiosity. *Geophysical Research Letters*, *45*(18), 9460–9470. https://doi.org/10.1029/2018gl079026
Palucis, M. C., Dietrich, W. E., Williams, R. M. E., Hayes, A. G., Parker, T., Sumner, D. Y., et al. (2016). Sequence and relative timing of large lakes in Gale crater (Mars) after the formation of Mount Sharp. *Journal of Geophysical Research: Planets*, *121*(3), 472–496. https://doi.org/10.1002/2015je004905
Park, S.-S. (2010). Effect of wetting on unconfined compressive strength of cemented sands. *Journal of Geotechnical and Geoenvironmental Engineering*, *136*(12), 1713–1720. https://doi.org/10.1061/(asce)gt.1943-5606.0000399
Parker, T. J., Anderson, R. C., Grant, J., & Heydari, E. (2023). Morphological and stratigraphic comparison of a ridge at the "marker band", Gale Crater, with a small Bay mouth bar in lake Bonneville, Utah. In *54th lunar and planetary science conference* (p. 2679).
Rampe, E. B., Bristow, T. F., Blake, D. F., Chipera, S. J., Vaniman, D. T., Achilles, C. N., & Sutter, B. (2023). Mineralogical evidence for environmental change in the clay-sulfate transition at Gale crater, Mars. In *54th lunar and planetary science conference* (p. 1554).
Rampe, E. B., Lapotre, M. G. A., Bristow, T. F., Arvidson, R. E., Morris, R. V., Achilles, C. N., et al. (2018). Sand Mineralogy within the Bagnold dunes, Gale Crater, as observed in situ and from orbit. *Geophysical Research Letters*, *45*(18), 9488–9497. https://doi.org/10.1029/2018GL079073
Rapin, W., Dromart, G., Clark, B. C., Schieber, J., Kite, E. S., Kah, L. C., et al. (2023). In situ evidence for sustained wet-dry cycling on early Mars. *Nature*, *620*(7973), 299–302. https://doi.org/10.1038/s41586-023-06220-3
Rapin, W., Dromart, G., Rubin, D., Deit, L. L., Mangold, N., Edgar, L. A., et al. (2021). Alternating wet and dry depositional environments recorded in the stratigraphy of Mount Sharp at Gale crater, Mars. *Geology*, *49*(7), 842–846. https://doi.org/10.1130/G48519.1
Roberts, A. L., Gupta, S., Dietrich, W. E., Edgar, L. A., Rapin, W., Banham, S. G., et al. (2023). What depositional processes and paleoenvironments formed the layered sulfate unit in Gale Crater, Mars? Insights from marker band valley. In *54th lunar and planetary science conference* (p. 2945).
Rudolph, A. (2024). Data for: An orbital comparison of a late mantling unit on Aeolis Mons with other erosion-resistant strata explored by MSL in Gale Crater, Mars. *Mendeley Data, V3*. (ArcGIS shapefiles of mapped units, CRISM ROIs used for spectral analyses, and derived spectral parameter data). https://doi.org/10.17632/mcdw3sp5vw.1
Rudolph, A., Horgan, B., Johnson, J., Bennett, K., Haber, J., Bell, J. F., et al. (2022). The distribution of clay minerals and their impact on diagenesis in glen Torridon, Gale Crater, Mars. *Journal of Geophysical Research: Planets*, *127*(10), e2021JE007098. https://doi.org/10.1029/2021je007098
Scudder, N. A., Horgan, B. H. N., Rampe, E. B., Smith, R. J., & Rutledge, A. M. (2021). The effects of magmatic evolution, crystallinity, and microtexture on the visible/near-infrared and thermal-infrared spectra of volcanic rocks. *Icarus*, *359*, 114344. https://doi.org/10.1016/j.icarus.2021.114344
Scuderi, L. A., Gallegos, Z. E., Newsom, H. E., Wiens, R. C., Grant, J. A., Gasnault, O., et al. (2019). An Amazonian groundwater Springline at Peace Vallis fan, Gale Crater; implications for a late period of surface water flow. In *50th lunar and planetary science conference* (p. 2714).
Scuderi, L. A., Nagle-McNaughton, T., Newsom, H. E., Williams, J., & Gallegos, Z. E. (2019). Evidence for resurfacing and subsequent groundwater Seepage peace Vallis channel, Gale Crater, Mars. In *Ninth International conference on Mars* (p. 6285).
Seelos, F. (2016). MRO CRISM targeted empirical record V1.0 [Dataset]. *NASA Planetary Data System*. https://doi.org/10.17189/1519573
Seelos, F. P., Seelos, K. D., Murchie, S. L., Novak, M. A. M., Hash, C. D., Morgan, M. F., et al. (2023). The CRISM investigation in Mars orbit: Overview, history, and delivered data products. *Icarus*, *2023*, 115612. https://doi.org/10.1016/j.icarus.2023.115612
Seelos, F. P., Viviano, C. E., Morgan, M. F., Romeo, G., Aiello, J. J., Murchie, S. L., & Team, C. (2016). CRISM hyperspectral targeted observation PDS product sets—TERs and MTRDRs. In *47th lunar and planetary science conference*.

Sheppard, R. Y., Milliken, R. E., Parente, M., & Itoh, Y. (2021). Updated perspectives and hypotheses on the Mineralogy of lower Mt. Sharp, Mars, as seen from orbit. *Journal of Geophysical Research: Planets*, *126*(2), e2020JE006372. https://doi.org/10.1029/2020je006372

Siebach, K. L., Baker, M. B., Grotzinger, J. P., McLennan, S. M., Gellert, R., Thompson, L. M., & Hurowitz, J. A. (2017). Sorting out compositional trends in sedimentary rocks of the Bradbury group (Aeolis Palus), Gale crater, Mars. *Journal of Geophysical Research: Planets*, *122*(2), 295–328. https://doi.org/10.1002/2016je005195

Stack, K. M., Grotzinger, J. P., Kah, L. C., Schmidt, M. E., Mangold, N., Edgett, K. S., et al. (2014). Diagenetic origin of nodules in the Sheepbed member, Yellowknife Bay formation, Gale crater, Mars. *Journal of Geophysical Research: Planets*, *119*(7), 1637–1664. https://doi.org/10.1002/2014je004617

Sun, V. Z., Stack, K. M., Kah, L. C., Thompson, L., Fischer, W., Williams, A. J., et al. (2019). Late-stage diagenetic concretions in the Murray formation, Gale crater, Mars. *Icarus*, *321*, 866–890. https://doi.org/10.1016/j.icarus.2018.12.030

Thompson, L. M., Kite, E. S., Grotzinger, J. P., Yen, A. S., Berger, J. A., Lewis, K. W., & Boyd, N. (2023). Investigation of the Gale Crater marker band (and beyond) with the Mars science Laboratory, alpha particle X-ray spectrometer. In *54th lunar and planetary science conference* (p. 2311).

Thomson, B. J., Bridges, N. T., Milliken, R., Baldridge, A., Hook, S. J., Crowley, J. K., et al. (2011). Constraints on the origin and evolution of the layered mound in Gale Crater, Mars using Mars Reconnaissance orbiter data. *Icarus*, *214*(2), 413–432. https://doi.org/10.1016/j.icarus.2011.05.002

Viviano, C. E., Murchie, S. L., Daubar, I. J., Morgan, M. F., Seelos, F. P., & Plescia, J. B. (2019). Composition of Amazonian volcanic materials in Tharsis and Elysium, Mars, from MRO/CRISM reflectance spectra. *Icarus*, *328*, 274–286. https://doi.org/10.1016/j.icarus.2019.03.001

Viviano, C. E., Seelos, F. P., Murchie, S. L., Kahn, E. G., Seelos, K. D., Taylor, H. W., et al. (2014). Revised CRISM spectral parameters and summary products based on the currently detected mineral diversity on Mars. *Journal of Geophysical Research: Planets*, *119*(6), 1403–1431. https://doi.org/10.1002/2014JE004627

Watkins, J. A., Grotzinger, J. P., Stein, N. T., Banham, S. G., Gupta, S., Rubin, D. M., et al. (2022). Burial and exhumation of sedimentary rocks revealed by the base stimson erosional unconformity, Gale Crater, Mars. *Journal of Geophysical Research: Planets*, *127*(7), e2022JE007293. https://doi.org/10.1029/2022JE007293

Weitz, C. M., Lewis, K. W., Bishop, J. L., Thomson, B. J., Arvidson, R. E., Grant, J. A., et al. (2022). Orbital observations of a marker horizon at Gale Crater. *Journal of Geophysical Research: Planets*, *127*(4), e2022JE007211. https://doi.org/10.1029/2022je007211

Weitz, C. M., Lewis, K. W., Kite, E., Dietrich, W. E., Thompson, L. M., O'connell-Cooper, C., et al. (2023). The marker band in Gale Crater. In *54th lunar and planetary science conference* (p. 1560).

Wiens, R. C., Maurice, S., Barraclough, B., Saccoccio, M., Barkley, W. C., Bell, J. F., et al. (2012). The ChemCam instrument suite on the Mars science Laboratory (MSL) rover: Body unit and combined system tests. *Space Science Reviews*, *170*(1–4), 167–227. https://doi.org/10.1007/s11214-012-9902-4

Wohletz, K. H., & Sheridan, M. F. (1983). Hydrovolcanic explosions; II, Evolution of basaltic tuff rings and tuff cones. *American Journal of Science*, *283*(5), 385–413. https://doi.org/10.2475/ajs.283.5.385

Yen, A. S., Ming, D. W., Vaniman, D. T., Gellert, R., Blake, D. F., Morris, R. V., et al. (2017). Multiple stages of aqueous alteration along fractures in mudstone and sandstone strata in Gale Crater, Mars. *Earth and Planetary Science Letters*, *471*, 186–198. https://doi.org/10.1016/j.epsl.2017.04.033